A Non-Invasive Method for Detecting a Deadly Form of Malaria: *Plasmodium Falciparum*

Undergraduate Honors Thesis

Brad Smith

Department of Mechanical Engineering
The Ohio State University
Spring 2014

_____

Prof. Vish Subramaniam, Advisor

This work was supported in part by the College of Engineering

Abstract

Malaria is an infectious disease transmitted by mosquitoes that affects 40% of the world's population, resulting in 300 to 500 million new infections yearly. Of the different types of malaria, *Plasmodium falciparum* (PF) is the most prevalent and deadly parasite in humans. While treatment is available, PF is often difficult to detect with a blood draw because the parasite sequesters in internal organs during various phases of its reproductive cycle. PF infects red blood cells, converting the hemoglobin in the red blood cells into iron rich particles called hemozoin. The hemozoin crystals can be as large as 1 μm in size and several clusters are stored in the food vacuoles of the parasite since they are toxic to the host and PF alike. PF is predominant in low and middle-income countries where pathologists and microscopes are not widely available to confirm the presence of this species of malaria. Consequently, an inexpensive, non-invasive, continuous, and direct indicator of PF is needed. The goal of this research is to exploit the paramagnetic properties of hemozoin and to develop a non-invasive, electromagnetic method of detecting infected red blood cells. An electromagnetic probe (EM probe) comprising of a dual coaxial coil is used to detect iron oxide particles by using sensitive lock-in amplification of detector voltage. Measurements with this probe are performed on iron oxide particles (less than 44 μm – 720 μm) before conducting measurements on PF food vacuoles. Results show that measurements of micron sized iron particles on the scale of less than 44 microns are repeatable. Preliminary measurements with food vacuoles trapped in small capillary tubes confirm feasibility of the method with indicated voltage differences of 44.7 ± 25.7 mV versus voltage readings for a control (capillary tube without trapped food vacuoles) of 16.2

± 4.3 mV with great potential for increased sensitivity. Preliminary optimization of the EM probe has resulted in greater sensitivity but considerable room for improvement still exists. This research demonstrates great promise for finding an alternative to existing methods (mainly peripheral blood draws) for the detection of PF. In addition to being non-invasive, the method described herein can provide detection results that can be interpreted in simple binary fashion (e.g. a readout red LED lighting up indicating the presence of infected cells and a green LED lighting up indicating no infection). This method therefore potentially lends itself to infected individuals being able to monitor themselves continuously throughout the day and getting timely treatment after confirmation, without the need for a peripheral blood draw, or the presence of a trained pathologist to interpret the microscopic examination of the drawn blood.

Acknowledgments

There are many people that made this research possible and provided much needed assistance along the way. I would first like to thank Prof. Vish Subramaniam. Prof. Subramaniam was always there to answer any questions, give any thoughts or ideas and guide me along throughout the entirety of my research process.

I would also like to thank Joe West who provided much needed assistance with all things electronic and was a wealth of knowledge and ideas whenever it was needed. Thank you to all of those in Prof. Subramaniam's lab who were always there to provide assistance and help me with problems. In particular, thank you to Emily Sequin, Travis Jones, and Scott Koch who helped to explain many things that I did not understand.

Thanks to Prof. Shaurya Prakash for serving on my undergraduate defense committee and his help in reviewing my thesis. Thanks to Dr. Mark Drew, Dawn Walker, and the Infectious Diseases Department for their help with supplying samples of food vacuoles for testing purposes. Thanks to Walter Green and the machine shop workers for their help whenever assistance was needed. Thanks to Daniel Roll for his sample of trapped food vacuoles used for testing. Thanks to Isaac Hong for his help with the camera microscope used for capturing images of test samples. Thanks to Prof. Robert Siston and those in the research class for the help in reviewing and critiquing my presentation.

A final thank you goes out to the College of Engineering and the department of Mechanical and Aerospace Engineering for their financial support and all of the faculty help throughout my undergraduate years at Ohio State.

Table of Contents

List of Figures

List of Tables

Chapter 1

Introduction

1.1) Background

Despite the fact that a treatment exists, malaria is currently one of the world's most fatal diseases resulting in over 1.2 million deaths a year [1]. Malaria is a mosquito-borne infection that is endemic to the tropics and low and middle-income countries (LMIC). Infection occurs when an infected female mosquito takes a blood meal from a human. An infection of the malaria parasite kills the host through consumption of the hemoglobin in the blood [2]. Around 40 percent of the world's population is at risk for acquiring malaria, affecting 300 to 500 million people each year. The most common age at death due to malaria is only 4 years of age with up to 23 percent of African infants being born with the malaria parasite [3]. Due to severe poverty, the most effective combative measures (bed nets, spray DDT and draining standing water) against mosquitoes that carry the deadly parasite are often not widely accessible in these countries.

1.1.1) *Plasmodium falciparum*

Of the four species of the parasite that cause malaria (*Plasmodium falciparum, Plasmodium malaria, Plasmodium ovale, and Plasmodium vivax*), the most dangerous is *Plasmodium falciparum* (PF). Almost all of the over 1 million deaths caused by malaria each year are from a PF infection [3]. Due to its complex life cycle, PF can be both hard to detect and to cure. PF goes through three major phases in its life cycle, the mosquito phase, the

human liver phase and the human blood phase. Upon injection through the saliva of an infected female mosquito, the infectious form of the PF parasite, known as sporozoites, enter the liver cells within minutes of injection. Within the liver, the sporozoites take on a new form and multiply rupturing the liver cells and the blood stage parasites, called merozoites, are released into the blood stream. These individual merozoites invade a red blood cell each, multiplying for two days before rupturing and releasing more merozoites to invade additional red blood cells [4]. This process continues and repeats itself resulting in the disease and often death if not properly treated.

It is in the human blood phase that the merozoites infect red blood cells, consuming the cell's cytoplasm and convert the hemoglobin in the red blood cell into iron rich particles called hemozoin. Hemozoin crystals are paramagnetic and produced by PF upon digestion of the hemoglobin [2]. The iron rich particles comprising the hemozoin crystals can be as large as 1 μm in size and several clusters are stored in food vacuoles of the parasite since they are toxic to the host and PF alike [5].

1.2) State-of-the-Art

There are currently two main ways to detect for malaria, and in particular *Plasmodium falciparum* (PF). These are a peripheral blood draw followed by analysis of red blood cells using an optical microscope, and the Rapid Diagnostic Test (RDT). An RDT is a quicker way to detect if certain types of malaria are present in the blood stream by placing a blood sample on a test card. After about 15 minutes, line indicators notify the user if any forms of malaria exist in the bloodstream [6]. While this process is quick, it does not eliminate the need for analysis using a microscope when the results of an RDT are negative

or inconclusive. The state of the art in detecting PF is microscopy, which requires a skilled technician or pathologist who must examine a blood sample from the patient under a microscope [7]. Figure 1 shows a typical microscope image of cells obtained from a blood sample infected with the PF parasite. Visible in the figure are the dark specks that are the hemozoin crystals within the food vacuoles of the parasite.

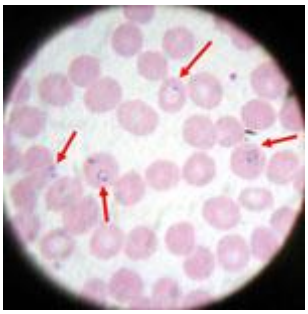

Figure 1: Blood smear of malaria (PF) infected red blood cells [6].

The disadvantages of microscopy are that these results are only as reliable as the individual or lab performing the analysis, and the fact that PF is not always present in the blood stream at the time of the peripheral blood draw. Microscopy is also impractical in rural areas of LMICs plagued by poverty, lack of equipment, lack of skilled labor, and lack of education.

Compounding the problem of detecting PF is that even when pathology facilities are available, sizeable errors in diagnosis do occur. False positive rates can be as high as 36% and false negatives 18% since PF is not always present in the blood stream when it sequesters in the liver and capillaries [8]. Therefore, there is a critical need for an inexpensive, accurate, easy to monitor, and non-invasive method of detecting PF.

1.3) Electromagnetic Detection

This work focuses on detecting paramagnetic particles on the scale of microns using an electromagnetic (EM) probe. An EM probe is comprised of coaxially wound inner and outer coils. The inner coil is used to produce the magnetic field that induces a voltage and current in the outer coil through inductive coupling. A change in the inductive interaction between the two coils occurs when a conductive or magnetic sample is placed inside the concentric coil arrangement causing a modification in the voltage and current characteristics of the outer coil. With the inner coil serving as the driver, the outer coil then acts as the detector.

Using a function generator to produce a voltage on the inner coil and thus driving a time varying current through the inner coil, results in a time varying magnetic field, according to Ampere's Law. This time varying magnetic field around the inner coil causes a current to be induced in the outer detector coil by Faraday's Law. With a time-varying current now in the outer coil, it also creates its own magnetic field that interacts with the inner coil. The sample placed inside these two coaxial, mutually coupled coils will alter this interaction, producing a small change in the voltage in the outer coil that can be detected using lock-in detection.

1.4) Review of Relevant Literature

The basis for the present work is on-going research at OSU on eddy current detection of cancer [9, 10, 11]. EM probes combined with lock-in amplification have shown that there is both a phase and magnitude difference between cancer bearing and normal tissue. The same ideas are used in this research to show that a minute paramagnetic

concentration of iron produces a detectable difference in both phase and magnitude. These differences are recognized as an altered detector coil voltage just as they are in the detection of cancer [9, 10, 11].

The magnetic properties of hemozoin have been described in previous studies. These are magnetic deposition microscopy, magneto-optic spectroscopic detection, and PCR (polymerase chain reaction) methods. Magnetic deposition microscopy has shown that bringing a magnet in proximity to a blood smear of malaria infected blood results in the parasite concentrating at a specific point on the slide where the magnetic field is greatest. This allows for just one area of the slide to be examined for any signs of infection [12]. Detection of malaria in suspensions with the eventual hope of detecting the parasite *in vivo* has been studied previously using a magneto-optic method. This method has been shown to be accurate when conducted on suspensions using the magnetic properties of hemozoin, but *in vivo* measurements have not yet been demonstrated [13]. The final method, PCR, uses saliva or dried blood in the detection of PF. This is also a way to detect PF non-invasively, but it is not a continuous type of detection, as a sample still needs to be acquired before this detection method can be utilized [14]. This research uses a few of the same concepts as some of those from previous work, but uses a new method in electromagnetic detection.

This thesis is organized as follows. The motivations for this research as well as its objectives are given in Chapter 2, followed by a detailed description of the design of the EM probe and associated experimental apparatus in Chapter 3. The experimental procedure is given in Chapter 4, followed by a discussion of the results in Chapter 5. The thesis then

concludes with a summary and conclusions of the present work as well as recommendations for further work in Chapter 6.

Chapter 2

Motivation and Objectives

2.1) Motivation

Malaria, and in particular, *Plasmodium falciparum* continues to be a big problem in the world today despite there being treatment available. This is due to many of the issues with the detection of PF as discussed in Chapter 1. Therefore, there is a critical need for an inexpensive, accurate, easy to monitor, and non-invasive method of detecting PF.

The paramagnetic properties of hemozoin can be utilized to develop an electromagnetic method of detecting infected red blood cells. The advantages of such an approach are that (1) it can be non-intrusive, i.e. blood need not be drawn, (2) its results can be interpreted in a simple binary fashion (e.g. red LED lighting up when infected cells are present and a green LED for no sign of infection), and (3) that a potentially infected individual can monitor themselves multiple times a day or even continuously without the need for a blood draw, and (4) that there is no need for a skilled pathologist to interpret the results. The end-goal of a PF detecting EM probe is shown schematically in Figure 2.

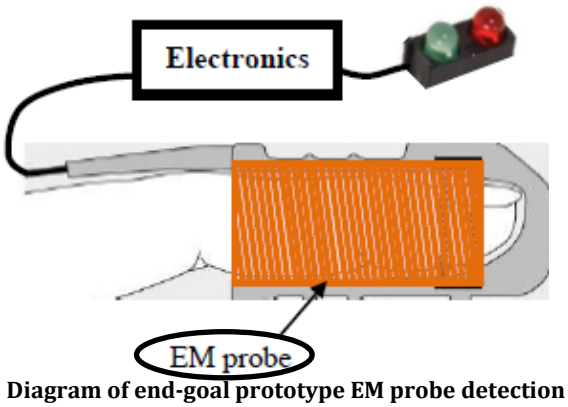

Figure 2: Diagram of end-goal prototype EM probe detection system

2.2) Objectives

There are three main objectives of this research. Each objective has the end goal of finding an alternative method to detecting PF that is easier to use, non-invasive and much more economical than the state-of-the-art detection procedures.

The first objective is to demonstrate the detection of iron oxide particles using an electromagnetic (EM) probe and lock-in detection. It is important to demonstrate that it is possible for the new method to detect iron oxide particles of substantial size before doing so on smaller particles of relevance to PF.

The second objective is to optimize the EM probe for detection of these smaller micron sized iron oxide particles. This is necessary to determine if the EM probe is not only capable of detecting iron oxide particles, but also capable of detecting particles that are on the same scale as those that will be found in the food vacuoles within the parasite. As described in Chapter 1, the food vacuoles contain the iron rich waste known as hemozoin, which is on the scale of one micron per each food vacuole. It is important to note that when a human host has contracted PF, the scale of hemozoin that must be able to be detected will be larger than one micron due to the number of PF infected red blood cells (level of parasitemia) in the body during an infection.

The final objective of this research is to demonstrate the feasibility of detecting these hemozoin particles in food vacuoles *in vitro* using the EM probe. This involves taking a pre-sorted sample of isolated food vacuoles from PF infected human blood (kindly supplied by Prof. Mark Drew and his group) and placing them inside a capillary tube which can be inserted into the EM probe. This experiment is used to demonstrate that the

hemozoin can be detected by the EM probe and will be a big step towards attaining the end goal of detecting PF infected blood *in vivo* using the EM probe.

Chapter 3

Experimental Apparatus and Design of the Electromagnetic Probe

The design methodology for developing an electromagnetic (EM) probe used in this research will be described in separate sections in this chapter. Details of the coil design and its fabrication are given. In addition, a description of the experimental apparatus is also provided.

3.1) Overview of the Design of the EM Probe

The EM probe developed in this work is based on the design methodology of an earlier series of probes labeled the A-series, which were used in the Applied Physics Laboratory for detection and imaging of cancer [10]. The A-series of coils comprised a primary side with 2 inner layers and an outer detector coil comprising 6 layers. For present purposes, the coil designed for detecting PF was wound as tightly as possible to the sample capillary tube in order to perform measurements on particles microns in size. It was presumed that the farther the sample is away from the detector coil, the less the signal that would be detectable.

With these design constraints in mind, PF1 was fabricated. PF1 consists of a concentrically wound dual coil that contains only 1 inner layer and 1 outer layer around a rod of spring steel of a slightly larger in diameter (1.45 mm) than that of the same glass capillary tubes (outer diameter of 1.10 mm) in which samples such as food vacuoles or micron sized iron oxide particles can be placed. This 1 by 1 coil design is a simplification of

the earlier coils used in the cancer detection studies. With only 1 inner layer and 1 outer layer, the coil is easier and less expensive to manufacture. The 1 by 1 coil has a much lower self-inductance (2.4 μH for the inner coil and 4.5 μH for the outer coil) compared to the earlier A-series (69.6 μH for the inner coil and 475.5 μH for the outer coil). The coil parameters of PF1 are given in Table 1 and its photograph is shown in Figure 3. Resistances and self-inductances were measured using an Extech Instruments LCR Meter (Model 380193). The capacitance of each coil cannot be measured accurately and was therefore inferred in the following manner. Using a previously developed circuit element model, the governing equations are numerically integrated to predict detector and primary coil voltages as a function of time [10]. These predictions are then compared to experimental measurements (e.g. see Fig. 4) made on each coil while varying the capacitance [10].

Table 1: PF1 EM Probe Parameters

Characteristic →	Coil Diameter (mm)	Length (mm)	# of Turns	Resistance (Ω)	Inductance (μH)	Capacitance* (pF)
Inner Coil	1.45	81.30	290	1.397	2.4	190
Outer Coil	3.25	81.30	290	1.661	4.5	190

*Capacitance estimated using derivation equations and matching to experimental oscilloscope trace

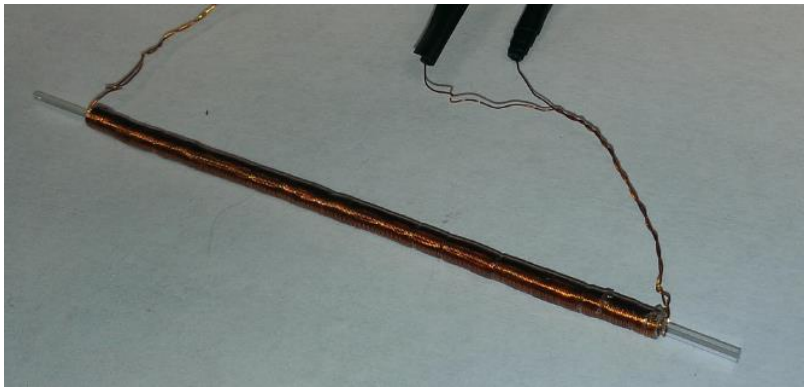

Figure 3: PF1 EM Probe

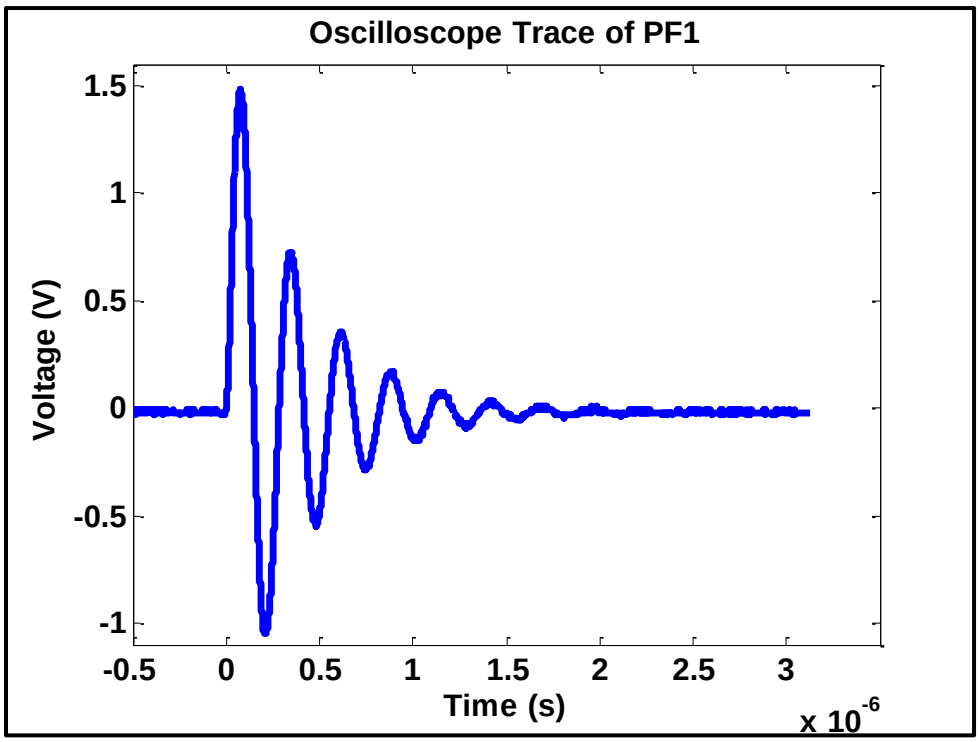

Figure 4: Typical voltage variation over a single cycle of the primary (inner) coil of PF1 displayed on an Oscilloscope

Initial measurements using PF1 were encouraging and are discussed in Chapter 5. However, certain flaws in its design had to be corrected. In particular, since the diameters of the capillary tubes containing the samples of iron oxide or food vacuoles were so close in dimension to PF1's inner diameter, there was a tendency to rub, resulting in unraveling of some of the windings of the inner coil of PF1. Therefore, a second coil, PF2, was designed and fabricated.

The second EM probe, PF2, was designed with a solid, non-conductive, hollow cylinder made of PVC, with an inside diameter of 1.45 mm and an outside diameter of 3.30 mm. All other parameters such as inductances and resistances were as close as possible to those of PF1. PF2 is also a 1 by 1 concentrically wound coil with the characteristics listed in Table 2. Resistances and self-inductances of the coils were measured using an Extech

Instruments LCR Meter (Model 380193). The capacitances were again found by matching the voltage traces predicted by numerical integration of the governing equations of a circuit element model and comparing them with the corresponding voltage traces measured on an oscilloscope [10]. A photograph of PF2 is shown in Figure 5 with its corresponding oscilloscope trace shown in Figure 6.

Table 2: PF2 EM Probe Parameters

Characteristic →	Coil Diameter (mm)	Length (mm)	# of Turns	Resistance (Ω)	Inductance (μH)	Capacitance* (pF)
Inner Coil	3.30	81.40	315	2.107	11.7	185
Outer Coil	4.25	81.40	315	2.342	15.1	185

*Capacitance estimated using derivation equations and matching to experimental oscilloscope trace

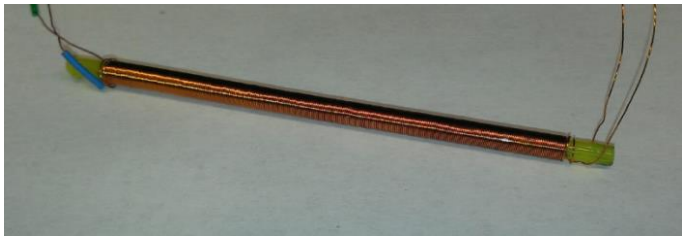

Figure 5: PF2 EM Probe

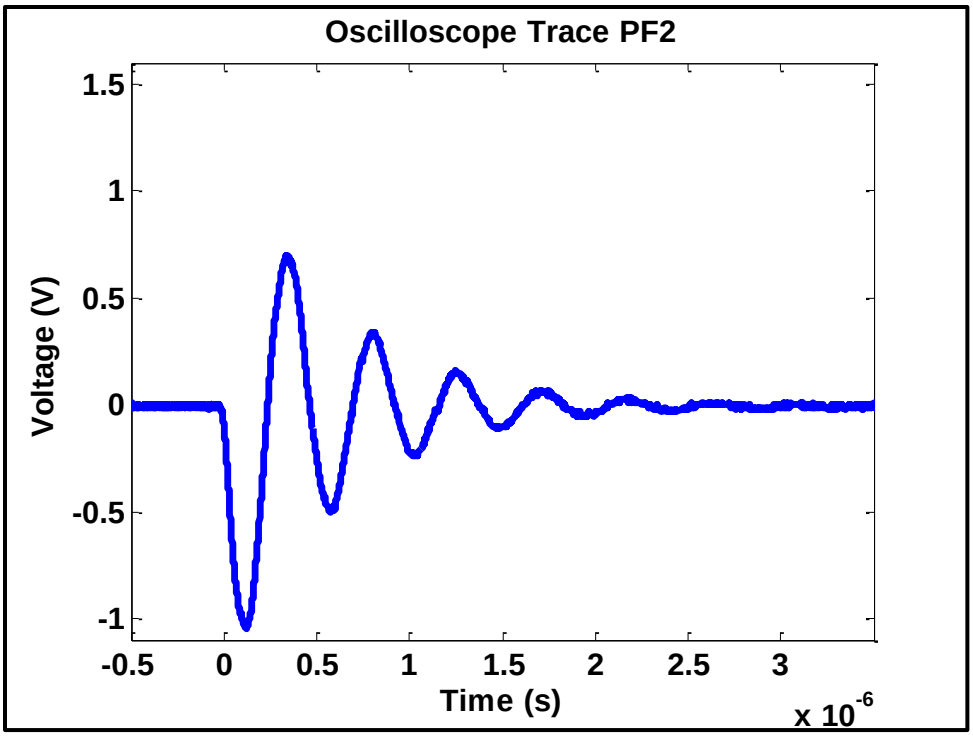

Figure 6: Typical voltage variation over a single cycle of the primary (inner) coil of PF2 displayed on an Oscilloscope

In the discussion of the results of measurements with both prototypes given in Chapter 5, it will be shown how the sensitivity differs between PF1 and PF2 as a result of differences in their diameters. Details of the fabrication of each probe is discussed next in the following section.

3.2) Overview of the Fabrication of the EM Probes

Each EM probe is fabricated using 32 American Wire Gauge (AWG) insulated copper wire (diameter of 0.202 mm). The inner layer is wrapped tightly by hand around the core used for each wire in a counterclockwise rotation as seen in Figure 7. For PF1, a mandrel made of spring steel with a diameter of 1.45 mm was used, which was then slid off, leaving an empty air core. PF2 was wrapped around a permanent core of hollow PVC plastic with an inner diameter of 1.45 mm and an outer diameter of 3.30 mm. After the first layer was

completed by carefully tightly winding so that there are no air gaps between windings, a layer of Clear Gloss 01, Sally Hansen Hard as Nails Color nail polish was applied to the entire outer layer of the inner coil. After allowing this layer of polish to dry, the outer layer was wound in the same fashion as the inner layer and in the same direction. The outer layer started at the same end as the inner coil start and again was wound by hand in a counterclockwise motion. It is again important to keep the windings as tightly packed as possible. Once the outer layer is complete, another layer of nail polish was applied to the outer layer of the outer coil. All loose ends of the coils were marked with either electrical tape or heat shrink to signify the end of the coil. This is important to note when finding those orientations of the coil that are most sensitive, as will be discussed in Chapter 5.

Figure 7: Diagram of beginning winding of the coil around a core. Coil wound counterclockwise when looking down the core from the start.

3.3) Experimental Apparatus

In this section, a description of the measurement system involving the EM probe is described. The measurement consists of first using a function generator to drive a transient current through the driver side of the EM probe. The induced current in the detector coil is then monitored as a voltage output to an oscilloscope or to a lock-in amplifier whose output in turn can be viewed on an oscilloscope. As a sample such as an iron oxide

specimen or iron-rich food vacuoles is placed inside the EM probe (i.e. inside the inner coil which is the primary coil), the mutual coupling between primary and detector coils is altered registering a change in the voltage recorded by the lock-in amplifier.

The 99 kHz sawtooth waveform at 7-10 Vpp voltage is imposed on the EM probe through a ballast resistor (800 – 1020 Ohms) on the primary coil, using a Hewlett Packard 33120A 15 MHz function/arbitrary waveform generator. As shown in Figure 8, a Stanford Research Systems, SR510 Lock-in Amplifier is used to measure the amplitude and phase of the voltage signal from the detector coil. The lock-in amplifier is used to extract otherwise small signals from noise. This lock-in generator DC signal is then output to a DSOX2014A, 100 MHz, 4 Channel Oscilloscope for data collection. The output on the oscilloscope is then recorded in .csv format to a flash drive to be used for analysis.

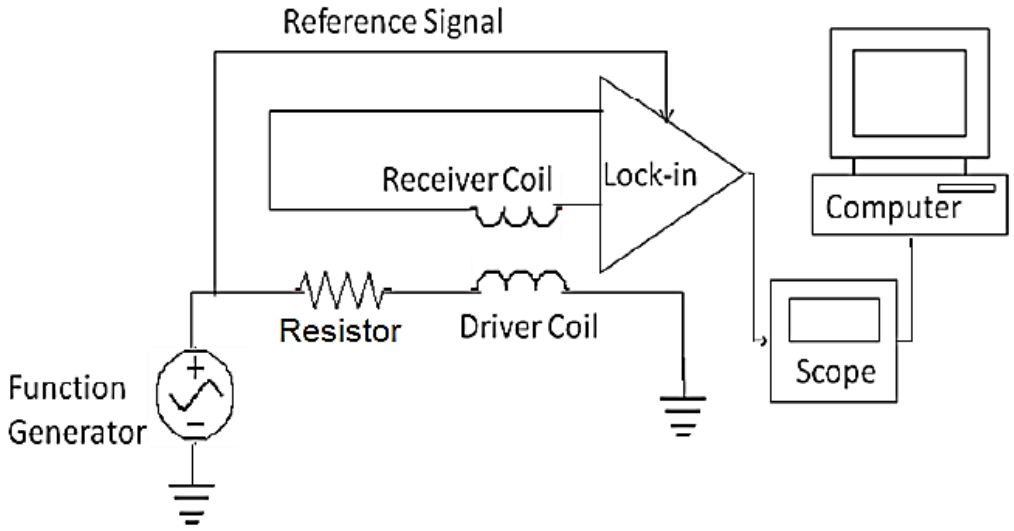

Figure 8: Experimental Setup for Data Collection

The EM probe is held in place by a non-conductive platform made out of acrylic sheets held together by nylon screws and nuts (Figure 9). The hand dial crank used to slide samples in and out of the EM probe is a tuner from an unused radio. The capillary tubes used to hold the samples were Kimble Chase 0.8 mm internal diameter, 1.1 mm outer diameter borosilicate glass tubes. The circuit board used to hard-wire the EM probe was a Multipurpose PC Board with 417 Holes (Model: 276-150). The complete measurement set up is shown in Figure 10.

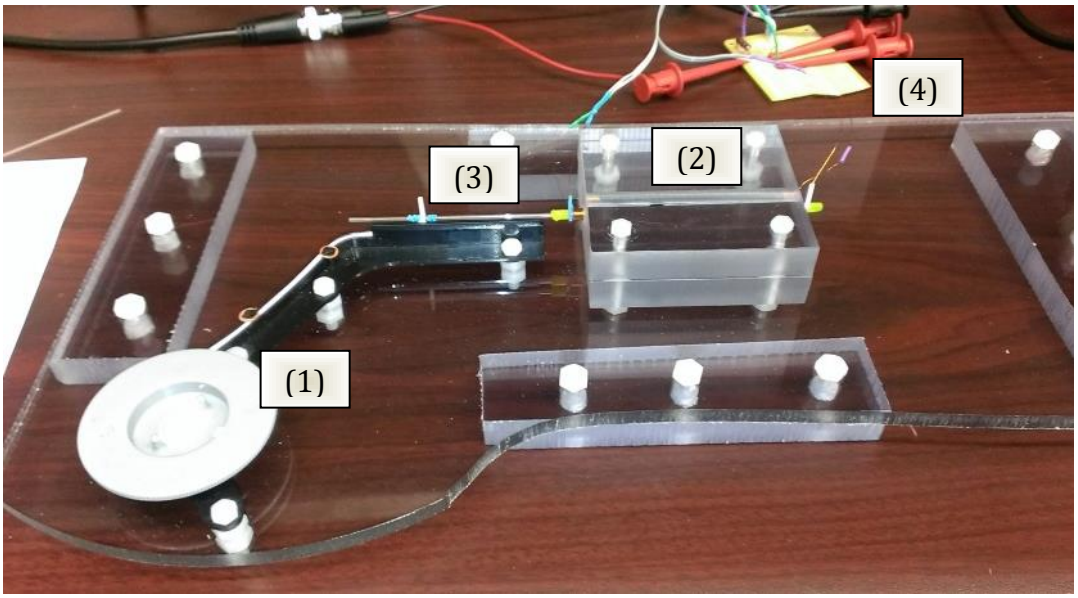

Figure 9: Stage: (1) Hand dial crank, (2) EM probe, (3) Capillary tube containing sample, (4) Hard wired multipurpose PC board

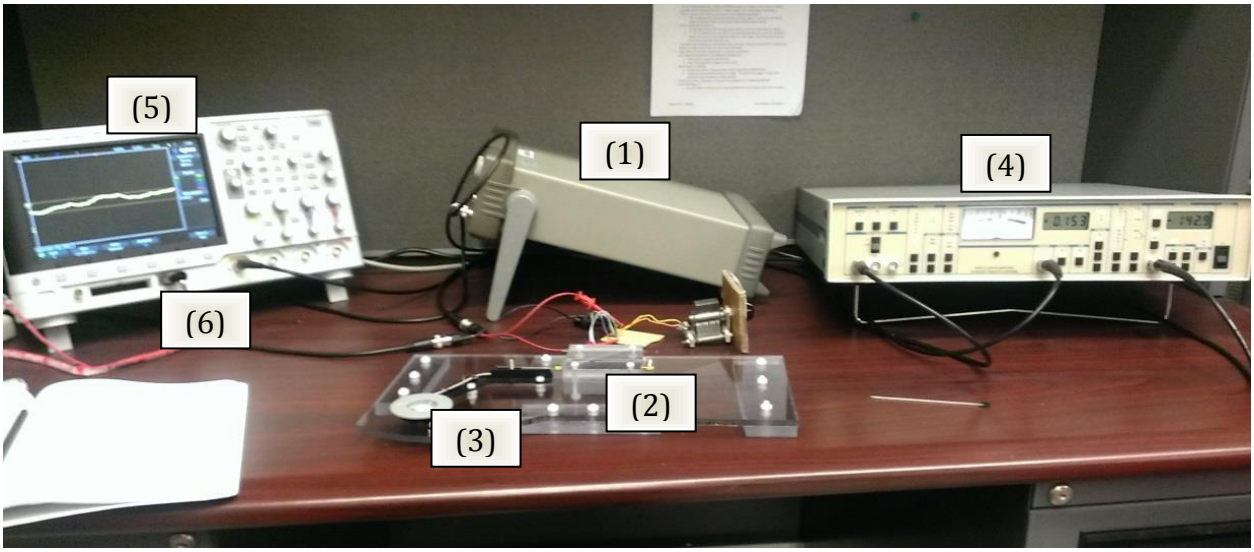

Figure 10: Complete data collection and EM probe measurement set-up: (1) Function Generator, (2) EM probe, (3) Stage, (4) Lock-In Amplifier, (5) Oscilloscope, (6) Flash drive for data storage

For measurement of particle mass, an Ohaus Analytical Plus AP250D balance was used. This scale has a 250 g weighing capacity and resolution of 0.1 mg. The iron particle samples were generated using Alfa Aesar iron powder, -325 mesh, reduced, 98% (metals basis). The following chapter describes the experimental procedure.

Chapter 4

Experimental Procedure

This chapter describes and outlines the procedures used to detect small iron oxide particles with the eventual aim of detecting the food vacuoles of PF. This section will describe the procedure for optimizing the probe, preparation of iron oxide samples, and the procedure for conducting the EM detection measurements on the iron particle samples.

4.1) Procedure for optimizing the EM probe

4.1.1) Procedure for selecting most sensitive coil arrangement

In earlier work in the Applied Physics Laboratory on detection of cancer, it was found that the sensitivity of a given probe could be increased by finding the optimum among four different arrangements of how the inner coil or the outer coil as the primary are connected to the external circuit. For the EM probe used in this research eight different arrangements were analyzed. The reason for examining the four additional arrangements with the outer coil acting as the primary side of the probe is to explore if there was an advantage to using the inner coil as the detector since the sample would be placed inside.

The coils are labeled according to the schemes shown in Figures 11 and 12. The beginning of the inner coil is labeled IS, with the inner coil end labeled IE. The outer coil follows the same nomenclature with the start of the outer coil labeled OS and the outer coil end labeled OE. In a 1 by 1 coil, either end could be labeled as the start or end but each wire was colored differently in order to distinguish them.

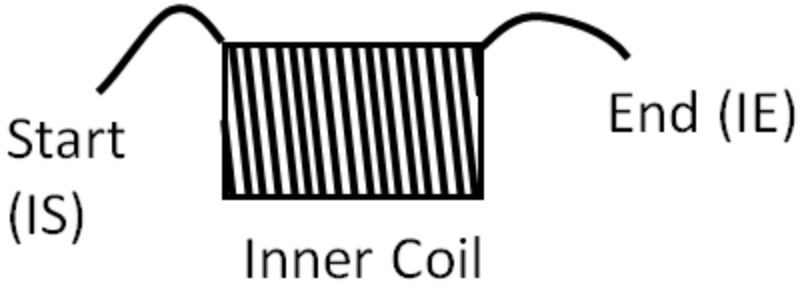

Figure 11: Inner coil of EM probe containing labels of each end of the coil

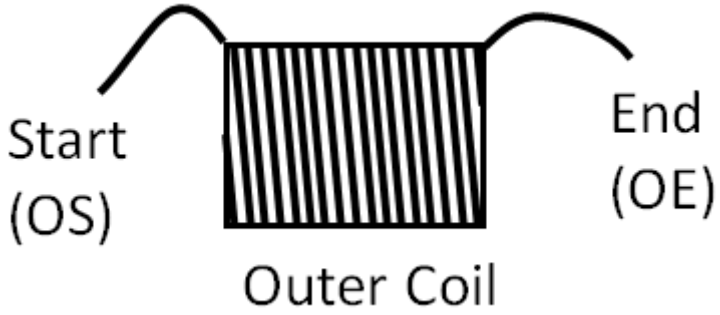

Figure 12: Outer coil of EM probe containing labels of each end of the coil

There are four arrangements explored with the inner coil connected to the function generator and switching the outer and inner coil leads. These arrangements are more easily understood as listed in Table 3, where the inner coil is the primary coil, and in Table 4 where the outer coil primary coil.

Table 3: Four coil arrangements when the inner coil driven by Function Generator

φ	IS+ IE-	IS- IE+
OS+ OE-	IS-OS	IE-OS
OS- OE+	IS-OE	IE-OE

Table 4: Four coil arrangements when the outer coil driven by Function Generator

φ	IS+ IE-	IS- IE+
OS+ OE-	OS-IS	OS-IE
OS- OE+	OE-IS	OE-IE

Measurements on the 659 μm solid iron particle were conducted using these eight unique arrangements to determine which arrangement yields the largest voltage difference and thus is most sensitive. The settings used for these measurements are listed in Table 5. The results from these measurements are discussed in Chapter 5.

Table 5: Instrument settings for coil arrangement experiments

Instrument	Option	Setting
Function Generator	Waveform	Sawtooth
	Frequency	99kHz
	Voltage	7Vpp
Lock-In Amplifier	Signal Input	A
	Sensitivity	2mV
	Dynamic Resolution	Norm
	All Offsets	Off
	All Expands	X1
	Display	$R\angle\phi$
	Mode	F
	Trigger	Sine
	Time Constant Pre	1s
	Time Constant Post	0.1s
	Bandpass Filter	Out
	Line Filter	Out
	Line x2 Filter	Out

4.1.2) Procedure for selecting optimum ballast resistance

The ballast resistance is an important part in the circuit system. The resistance that is connected between the function generator and the EM probe (Figure 8) serves to keep the current in the circuit constant. If the ballast resistance is too high, current is reduced and the magnitude of the voltage differences between sample and null (no sample) decreases. If the ballast resistance is too low, sensitivity to a sample can be reduced as inductance begins to dominate. For these reasons, it is important to have a ballast resistance that is ideal for the EM probe to be able to detect small amounts of iron.

To determine which ballast resistance will be the best, arrays of different resistances are individually placed in the circuit and an oscilloscope trace is taken of the voltage variation over a single cycle of the optimum coil arrangement as found in the previous section. These oscilloscope outputs are analyzed to find the effect of the added

resistance and if it is destroying peaks or causing too little of a voltage difference between peaks. The settings used for these measurements are listed in Table 6. The voltage was increased from 7 Vpp to 10 Vpp to allow for a larger voltage drop of the Sawtooth wave resulting in higher dB/dt and increasing the induced voltage in the detector coil by Faraday. The results of these measurements are discussed in Chapter 5.

Table 6: Instrument settings for ballast resistance experiments

Instrument	Option	Setting
Function Generator	Waveform	Sawtooth
	Frequency	99 kHz
	Voltage	10 Vpp

4.1.3) Procedure for finding optimum external capacitance

In earlier work in the Applied Physics Laboratory, it was discovered that the sensitivity of a given EM probe can be enhanced by adding a small amount of capacitance in the external circuit of the detector, regardless of any variability introduced during the fabrication process of the coil. In an effort to optimize PF1 and PF2 to be able to detect small iron islands such as the food vacuoles of PF, capacitance was added in a systematic manner to the external circuit of the detector coil. The procedure by which this was done is described here and the results are discussed in detail in Chapter 5.

First, a variable capacitor ranging from 10 pF to 100 pF was hardwired into the multipurpose board (Figure 13). This variable capacitor was easily adjusted using the dial knob shown in Figure 14. Using the 659 μm particle as the sample, the variable capacitor was adjusted in 10 pF increments (starting from 10 pF) and measurements were recorded with and without the sample.

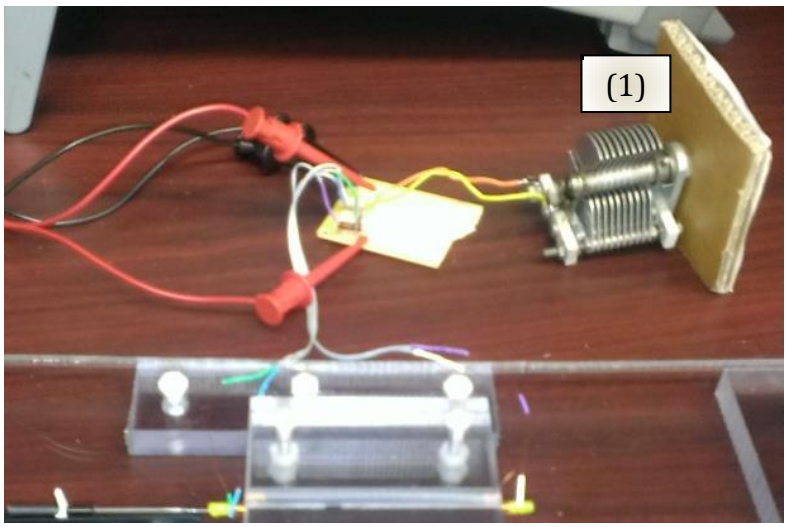

Figure 13: Hardwired variable capacitor (1)

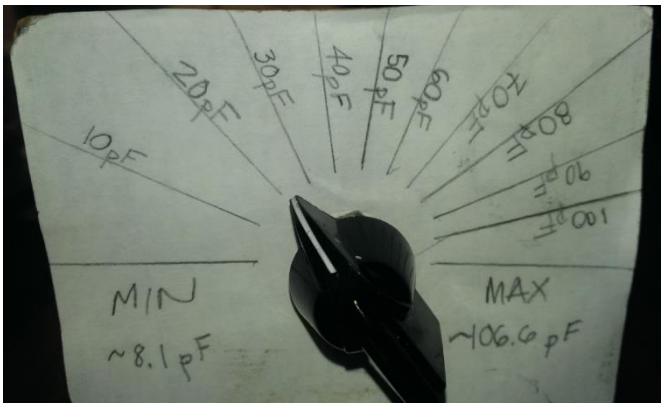

Figure 14: Dial knob indicator for variable capacitor

There were four variable external capacitance experiments conducted each with a different ballast resistance (1020 Ω, 800 Ω, 390 Ω, and 2200 Ω). This was an experiment to see how the variable external capacitance affected the sensitivity while also analyzing how the varying ballast resistance affected the sensitivity as well. The settings for the external capacitance experiments are given in Table 7.

Table 7: Instrument settings for coil arrangement experiments

Instrument	Option	Setting
Function Generator	Waveform	Sawtooth
	Frequency	99kHz
	Voltage	10Vpp
Lock-In Amplifier	Signal Input	A
	Sensitivity	2mV
	Dynamic Resolution	Norm
	All Offsets	Off
	All Expands	X1
	Display	$R\angle\phi$
	Mode	F
	Trigger	Sine
	Time Constant Pre	1s
	Time Constant Post	0.1s
	Bandpass Filter	Out
	Line Filter	Out
	Line x2 Filter	Out

4.2) Preparation of iron oxide samples

Experiments for optimizing the EM probe were conducted on a 659 μm sized solid iron (oxide) particle. Additional measurements to explore the sensitivity of the EM probe to small particles were made on other samples of iron oxide particles generated using the procedure described in this section.

First, the mass of all the capillary tubes used for samples were measured using the Ohaus scale. Each tube was stored separately and labeled. Iron oxide powder (Alfa Aesar, 325 mesh, less than 44 μm in size per particle) was used to produce samples of different amounts and agglomerated sizes within the capillary tubes. The powder was placed into a small glass container with deionized water and then shaken by a vortex mixer until thoroughly mixed. Allowing about a minute for the larger particles to settle to the bottom of the glass container, the 0.8 mm internal diameter capillary tubes were inserted at various

depths inside the mixture to provide several different concentrations. Through capillary action samples of iron particles and deionized water were drawn into the tubes. These capillary tubes with the samples were then placed in a fume hood to allow for increased air flow and the water was allowed to evaporate. Once the samples were completely free of any water, their masses were measured again. The difference in mass between the tube with the sample and just the tube alone was recorded as the mass of the sample alone. Table 8 lists the mass, volume and estimated equivalent spherical diameter of the samples. All microscope images of the iron samples are given in Appendix A.

Table 8: Iron Particle Samples

Sample	Mass (±0.2E-4 g)	Volume (μm^3)	Estimated Equivalent Diameter** (μm)
Empty Tube	-	-	-
Particle	11.(8)E-4	149.9E+06	659.0
1*	(0.04E-4)	0.5E+06	95.8
2	0.(2)E-4	2.5E+06	169.3
3	0.(5)E-4	6.4E+06	229.8
4*	(0.04E-4)	0.5E+06	98.7
5*	(0.05E-4)	0.6E+06	104.8
6	0.(8)E-4	10.2E+06	268.7
7	5.(4)E-4	68.6E+06	507.8
8	1.(2)E-4	15.2E+06	307.6
9	1.(1)E-4	14.0E+06	298.8

*Volume estimated using microscope images
**Assumption: All particles combined equal perfect sphere

The mass was found using the scale for all samples but 1, 4 and 5. With a mass, the volume could be found knowing that the density of the iron powder used is 7.874 (10^{-12}) g/μm^3 [Alfa Aesar]. For samples 1, 4, and 5, the volume was estimated using the

microscope images of the iron particles as the scale did not read any change in mass and then the mass was estimated using the density. The estimated equivalent diameter is an assumption that all of the particles are combined into one perfect sphere to make it easier to compare between the samples. The diameter was found using the volume and finding the diameter of a sphere:

$$V_{sphere} = \frac{4}{3}\pi r^3 \Rightarrow D = 2\left(\sqrt[3]{\frac{V_{sphere}}{\frac{4}{3}\pi}}\right)$$

4.3) Experimental procedure for measurements on iron particle and food vacuole samples

Figure 15 shows a close up of the apparatus and fixture used to slide the capillary tubes containing the samples into the EM probe. The blue heat shrink tube was used to hold the capillary tube rigidly as it was slid into the EM probe. In a later improvement on this fixture, electrical tape was applied directly to the capillary tube containing the sample. This used the same idea of allowing the dial indicator to move the sample in and out of the EM probe without physically touching the sample or EM probe. This set-up is shown in Figure 16.

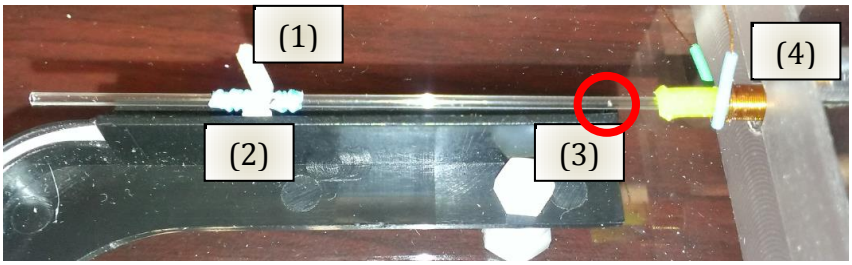

Figure 15: Capillary tube containing sample: (1) Dial indicator, (2) Heat shrink used for position the tube, (3) Sample – 659 μm particle, (4) EM probe

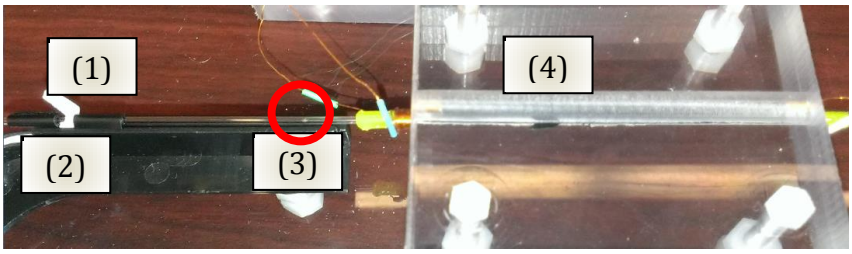

Figure 16: Capillary tube containing sample: (1) Dial indicator, (2) Electrical tape used for position the tube, (3) Sample – 659 μm particle, (4) EM probe

Chapter 5

Experimental Results

The preliminary experiments with prototype PF1 are discussed first along with a comparison of prototype PF2. Section 5.2 describes the experiments conducted to optimize the EM probe, and measurements on micron sized iron oxide samples and food vacuoles are discussed in Section 5.3.

5.1) PF1 voltage difference with 659 μm iron particle

Early experiments using the prototype PF1 were conducted with the IS-OS coil arrangement in which the current was driven through the start of the inner coil with the signal detected through the outer coil by the lock-in amplifier (the start of the outer coil or OS is connected to the input of the lock-in amplifier while the end of the outer coil, OE is grounded). While this orientation gives the largest output signal, it is not necessarily optimal for having the largest difference in signal between sample and null. This was taken into account with prototype PF2 as described in Section 5.2

In preliminary experiments, the solid 659 μm iron particle was used as the sample to determine whether the detectable signal was larger when the sample was placed outside of the probe (PF1) or when it was placed inside the probe. Six different trials were conducted to ensure that the measurement was repeatable. For each trial, the sample was completely outside of the coil and was slid inside using the stage described in Chapter 3.

This experiment was conducted with a 1020 Ω ballast resistance and the instrument settings are listed in Table 9 with the results shown in Figure 17.

Table 9: Instrument settings for PF1 experiment on a 659 μm iron particle

Instrument	Option	Setting
Function Generator	Waveform	Sawtooth
	Frequency	99kHz
	Voltage	7Vpp
Lock-In Amplifier	Signal Input	A
	Sensitivity	2mV
	Dynamic Resolution	Norm
	All Offsets	Off
	All Expands	X1
	Display	$R\angle\phi$
	Mode	F
	Trigger	Sine
	Time Constant Pre	1s
	Time Constant Post	0.1s
	Bandpass Filter	Out
	Line Filter	Out
	Line x2 Filter	Out
	Reference	-48.4°

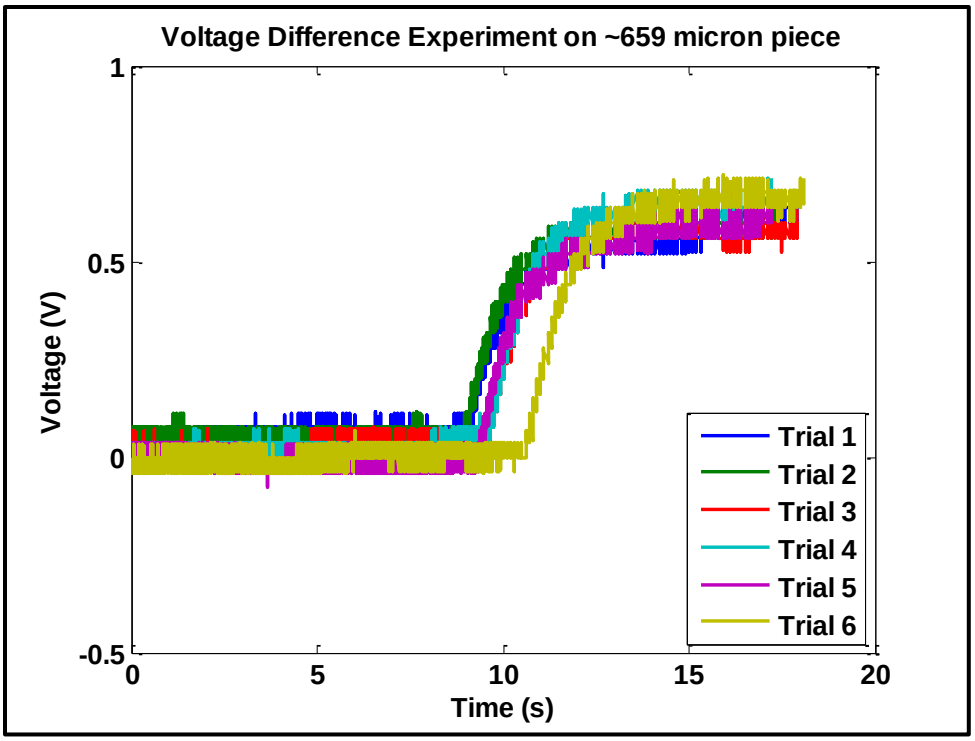

Figure 17: Oscilloscope output showing the voltage difference when a 659 μm iron particle is placed inside PF1

As can be seen from Fig. 17, the average voltage difference between sample and null is 0.6041 volts with a standard deviation of 0.0418 volts. Figure 17 shows that the results are very reproducible and the standard deviation helps to solidify this claim. This signal is quite substantial as the sensitivity setting on the lock-in amplifier can be reduced resulting in much higher sensitivity with the probe yet to be fully optimized. However, due to the inner diameter of PF1 being only 0.35 mm in diameter larger than the capillary tubes that were slid inside it, the insulation layer was beginning to be damaged and a second coil was made. The second prototype PF2 was therefore fabricated, optimized, and henceforth the results presented in this thesis are with PF2.

5.2) Prototype PF2

Eight unique orientations of PF2 were analyzed to determine which was the most sensitive and thus the best arrangement to use for measurements on the micron sized iron particles and food vacuoles. Oscilloscope traces were taken for each arrangement. The recorded voltage traces for each orientation for one period are shown in Figures 18 and 19.

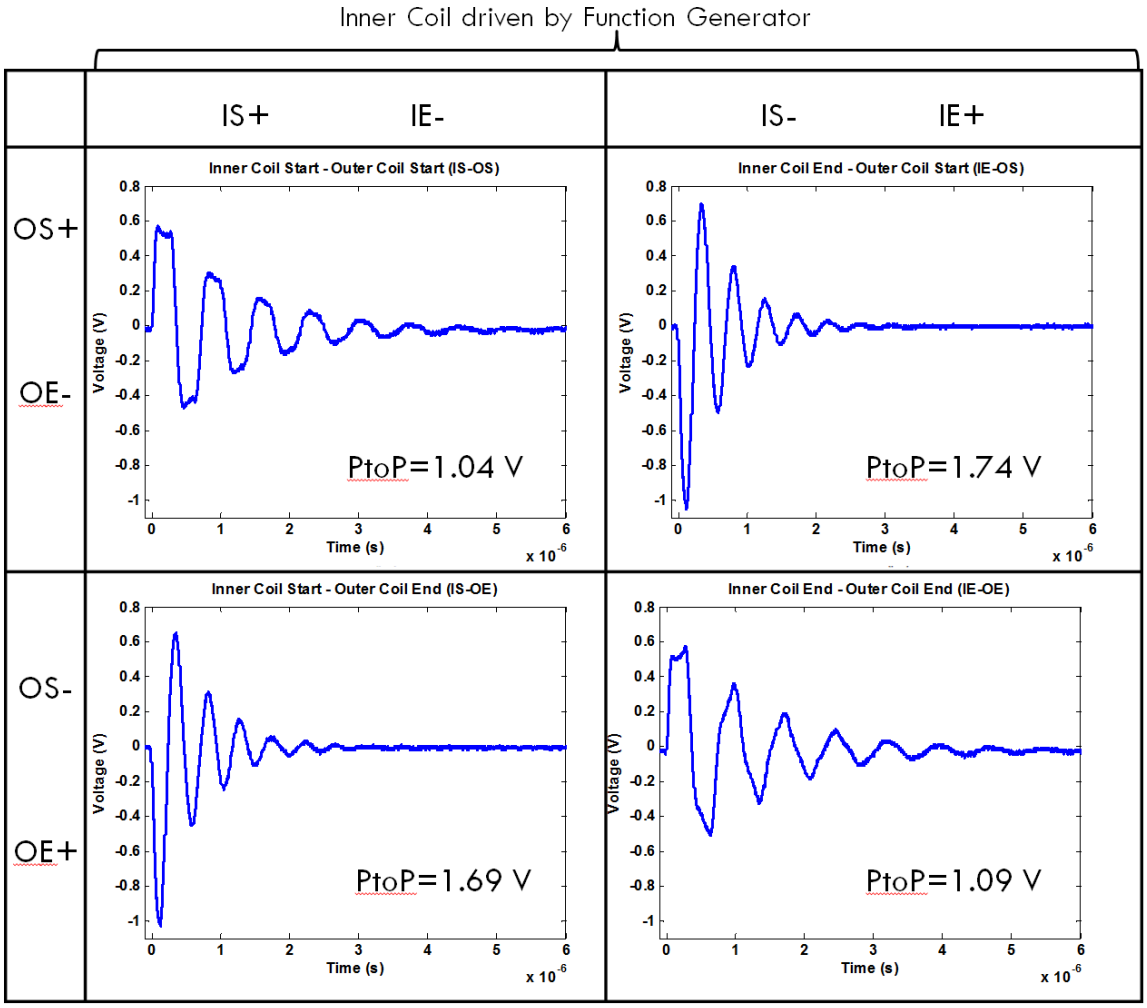

Figure 18: PF2 oscilloscope traces for each coil arrangement with inner coil as the driver

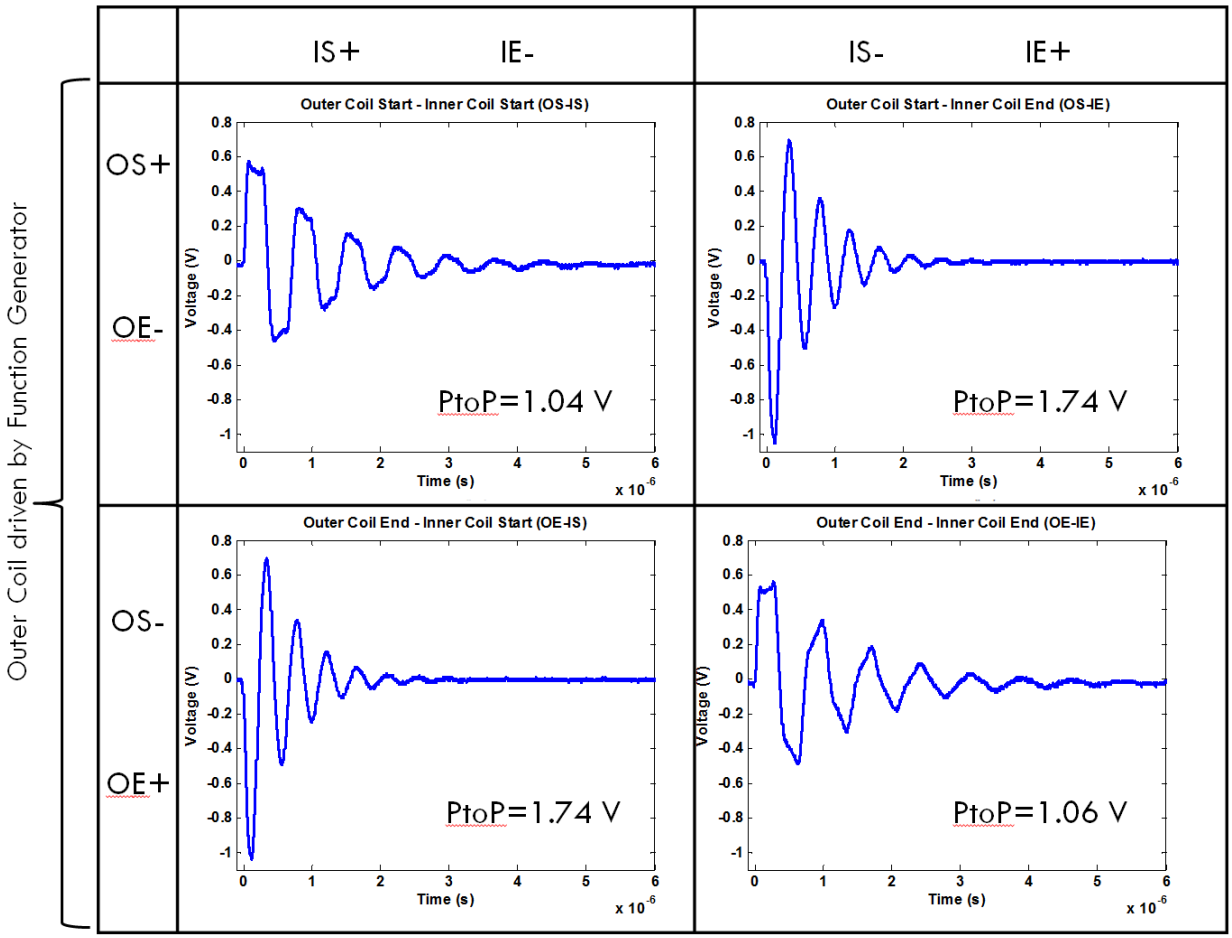

Figure 19: PF2 oscilloscope traces for each coil arrangement with outer coil as the driver

From the results shown in Figs. 18 and 19, it can be seen that the arrangements IE-OS, OS-IE, and OE-IS all result in the same Peak to Peak voltage (PtoP) as measured by the oscilloscope of ~1.74 V. Each of the eight arrangements were then used to measure the difference in signal between sample and null for the 659 μm particle. The results of these experiments for each arrangement are given in Tables 10 and 11.

Table 10: PF2 voltage differences (in mV), between sample present and null, with the inner coil as the driver

φ	IS+ IE-	IS- IE+
OS+ OE-	IS-OS **57.650±2.631** (Ref: +31.4°)	IE-OS **130.375±3.221** (Ref: -165.7°)
OS- OE+	IS-OE **84.514±2.093** (Ref: -159.4°)	IE-OE **98.314±5.943** (Ref: +27.5°)

Table 11: PF2 voltage differences (in mV), between sample present and null, with the outer coil as the driver

φ	IS+ IE-	IS- IE+
OS+ OE-	OS-IS ***7.734±4.379*** (Ref: +32.4°)	OS-IE ***47.696±5.894*** (Ref: -157.2°)
OS- OE+	OE-IS **42.855±7.933** (Ref: -158.0°)	OE-IE **118.930±5.158** (Ref: +30.3°)

Each arrangement is labeled, and average voltage difference (in mV) between sample and null along with the corresponding standard deviation is given. The reference phase (in degrees) as read on the lock-in amplifier is also included for uses in repeating this experiment. From these results, it is noticed that the IE-OS arrangement produces the greatest voltage difference and is therefore considered the most sensitive arrangement. The oscilloscope output as read from the lock-in amplifier for the IE-OS orientation is shown in Figure 20.

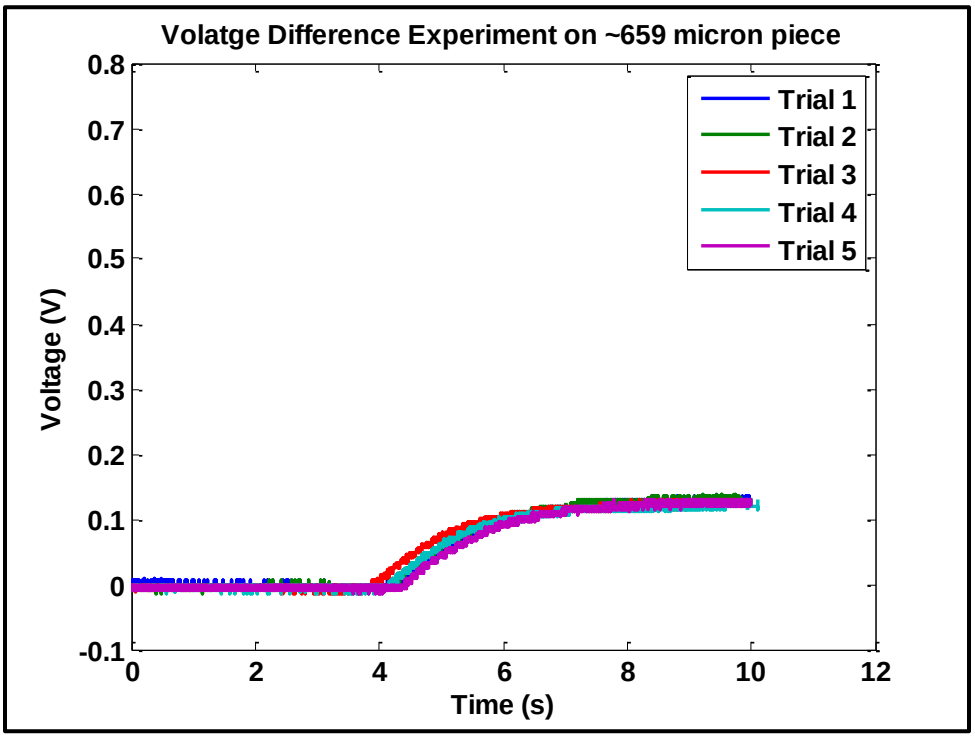

Figure 20: Oscilloscope output showing the voltage difference when a 659 μm iron particle is placed inside PF2 for the IE-OS arrangement

The average voltage difference between sample and null (for the 659 μm particle) for the most sensitive arrangement of PF2, labeled as IE-OS, was measured to be 0.1304 V with a standard deviation of 0.0032 volts. Since all of the parameters for the function generator

(input) and for the lock-in amplifier (output) were maintained the same as the preliminary measurements conducted with PF1 and given in Table 9, the performance of PF1 and PF2 can be directly compared. When comparing the average voltage difference it is noticed that PF1 (0.6041±0.0418 V) produces an average voltage difference over 4.5 times larger than the most sensitive arrangement of PF2 (0.1304±0.0032 V). This is most likely due to the smaller diameter of PF1. The EM probe inner coil for PF2 is 0.925 mm further away from the sample than that of PF1 which is about 0.325 mm away from the sample. This places the inner coil of PF2 over 3 times further away from the sample than PF1, likely resulting in the decrease in signal for PF2.

5.3) Optimum ballast resistance for PF2

The purpose of adding a ballast resistance is to enable the current on the primary side to follow the applied voltage as much as possible. There is a trade-off between the amount of current that is allowed through the primary coil with the greater that current, the greater the voltage difference between sample and null obtained on the detector coil, but if there is not enough resistance, the characteristics of the EM probe are distorted as inductance begins to take over leading to lower sensitivity. This is evident when six different ballast resistances were tested to determine which would be the optimal one to use. The resistors used were the original 1020 Ω, along with five others; 200 Ω, 450 Ω, 630 Ω, 677 Ω and 800 Ω. Using the optimum coil arrangement with the specified ballast resistance, oscilloscope traces were obtained and are given in Appendix B.

After analyzing these traces, it was decided that anything below a ballast resistance of 800 Ω resulted in distortion of the detector coil voltage and likely lower detectable

signal. In addition, since the smallest resistor without destroying the signal is desired, the 800 Ω resistor was selected over the 1020 Ω resistor. Additional checks with ballast resistance were conducted at the same time as varying the external capacitance on the detector side. These results are discussed in the following section.

5.4) Optimizing PF2 with externally added Capacitance

Four experiments varying external capacitance using unique ballast resistances (390 Ω, 800 Ω, 1020 Ω, and 2200 Ω) were conducted. These measurements were conducted on the 659 μm iron particle. The external capacitance was varied using a variable capacitor, which allowed measurements from 10 pF to 100 pF. A measurement was performed with 0 pF, with the variable capacitor removed. The results of each of these experiments is shown in Figure 21. These results are also given in tabulated form in Appendix C.

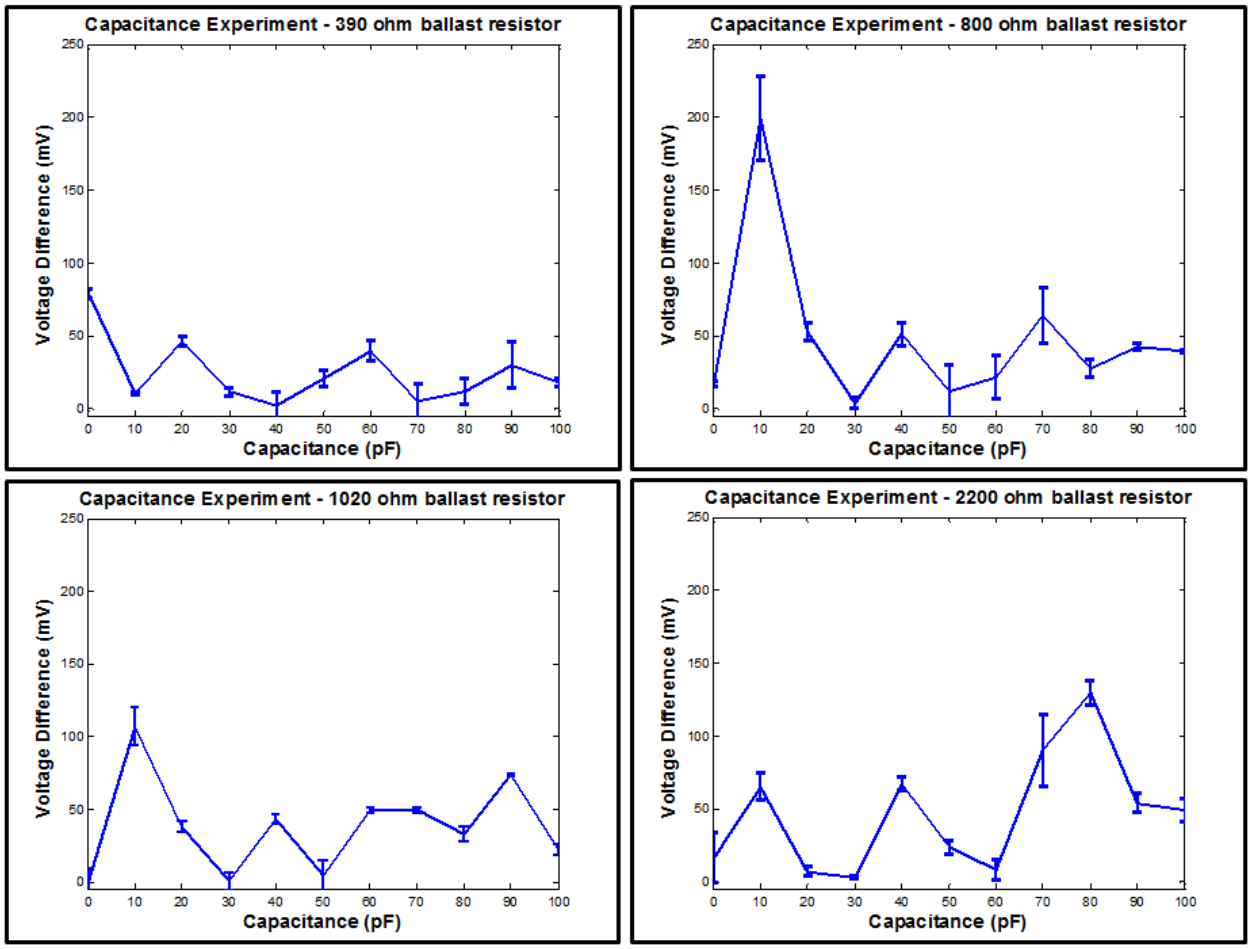

Figure 21: PF2 capacitance experiment for all four ballast resistors

It was found that indeed, adding external capacitance on the detector side of the circuit does improve the sensitivity of the detection. Only the experiment with a 390 Ω ballast resistance did not show improvement when adding external capacitance. Each of the 800 Ω, 1020 Ω, and 2200 Ω experiments have settings where the added external capacitance greatly increases the signal at a particular value of the external capacitance. The 390 Ω resistor was tested to observe what would happen to the sensitivity when the ballast resistance was cut in half. When this did not produce better results than with the 800 Ω resistor, the ballast resistance was doubled to that of the original ballast resistance of 1020 Ω, at 2200 Ω. This was also a check to determine which ballast resistance would be

the optimal one following the previous experiment described in Section 5.3. These results show that the initial selection of 800 Ω for the ballast resistance was indeed the most optimal resistor of those tested.

All aforementioned optimizations were conducted with the lock-in amplifier's Dynamic Reserve setting at Normal. The configuration with an 800 Ω ballast resistance was then examined with the lock-in amplifier dynamic reserve setting set to Low. The dynamic reserve adds a bandpass filter of 20 dB when the setting is changed from "Low" to "Normal". For a dynamic reserve of Low, the bandpass filter is 20 dB and for Normal it is 40 dB. At a Low setting, it is expected for the sensitivity to increase as the filter is not as sharp, but this will also result in an increase in the noise. In addition, at this Low setting, only so much capacitance can be added to the detector external circuit without overloading the Lock-in amplifier. For the case with the 800 Ω ballast resistor, the optimum external capacitance was found to be about 25 pF without overloading the lock-in amplifier. The results of optimizing for external capacitance are shown in Figure 22 and the same results tabulated are given in Appendix C.

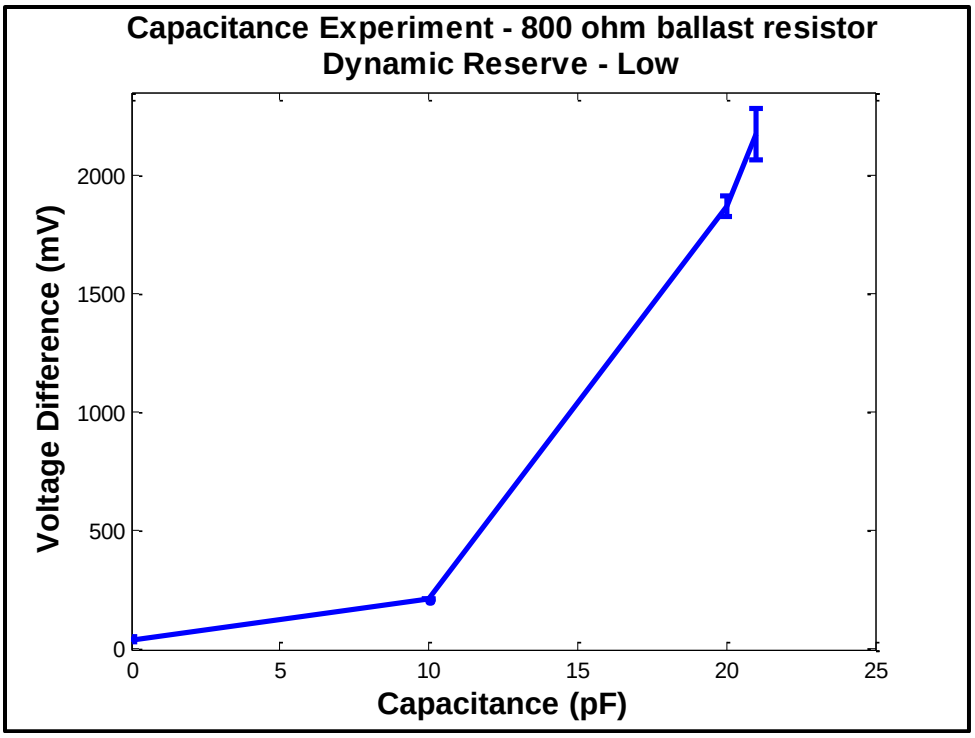

Figure 22: PF2 capacitance experiment for 800 Ω resistor on Dynamic Reserve of Low

In summary, the measurements on the 659 μm particle show great increase in sensitivity with about 20 pF of external capacitance added to the detector coil circuit when the Dynamic Reserve is set to Low. This increase results in a signal that is 10 times larger than that of any voltage difference observed with the Dynamic Reserve offset at Normal. Due to this substantial increase in signal difference between sample and null, this configuration was chosen for measurements on the food vacuoles isolated from PF and trapped in a capillary tube.

5.4.1) Preliminary measurements on PF Food vacuoles using Prototype PF2

Food vacuoles isolated from PF infected human blood (obtained from Prof. Mark Drew and Dawn Walker of the Department of Internal Medicine at The Ohio State University) were trapped inside a thin capillary tube by applying a strong magnetic field of ~ 35 T in less than 10 pulses lasting a few microseconds (trapped by Joe West and Daniel Roll of the Department of Mechanical Engineering at The Ohio State University). This form of trapping the food vacuoles resulted in two agglomerations as can be seen in Figures 23 and 24.

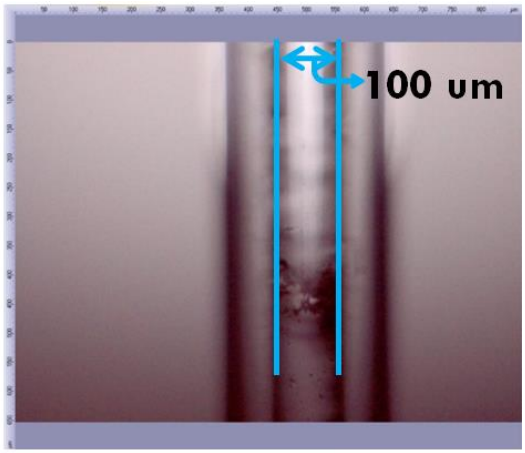

Figure 23: Food vacuole agglomeration 1 as seen under a compound microscope at 200x magnification

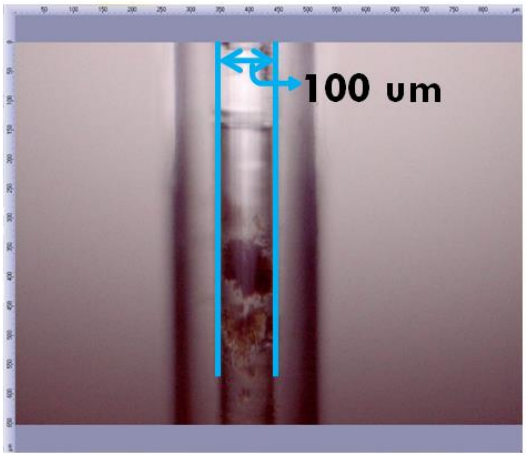

Figure 24: Food vacuole agglomeration 2 as seen under a compound microscope at 200x magnification

These food vacuoles were estimated to have a volume of about 15710 μm^3 for agglomeration 1 (Fig. 23) and 47120 μm^3 for agglomeration 2 (Fig. 24). This results in a total volume of about 62830 μm^3 in the test section within the EM probe and if this is considered to be one spherical mass, the estimated equivalent diameter of all the food vacuoles combined would be about 50 μm. With the sample thus identified and sized, the settings used for detection experiments with the EM probe are given in Table 12.

Table 12: Instrument settings for PF2 experiment on ~50 μm food vacuoles

Instrument	Option	Setting
Function Generator	Waveform	Sawtooth
	Frequency	99kHz
	Voltage	10Vpp
Lock-In Amplifier	Signal Input	A
	Sensitivity	2mV
	Dynamic Resolution	Low
	All Offsets	Off
	All Expands	X1
	Display	$R\angle\phi$
	Mode	F
	Trigger	Sine
	Time Constant Pre	3s
	Time Constant Post	0.1s
	Bandpass Filter	Out
	Line Filter	Out
	Line x2 Filter	Out

These settings are nearly identical to those given at the end of section 5.4 where the EM probe was found to be most sensitive with an added external capacitance of a little over 20 pF on a Dynamic Reserve setting of "Low" on the lock-in amplifier. Only the pre time constant is changed from 1 second to 3 seconds. This is done to reduce the noise so that when the signal is zoomed in on the oscilloscope, the fluctuations are reduced. Measurements are conducted on an empty glass capillary tube as control as well as on food

vacuoles, and these results are shown in Figures 25 and 26, and in tabulated form in Table 13.

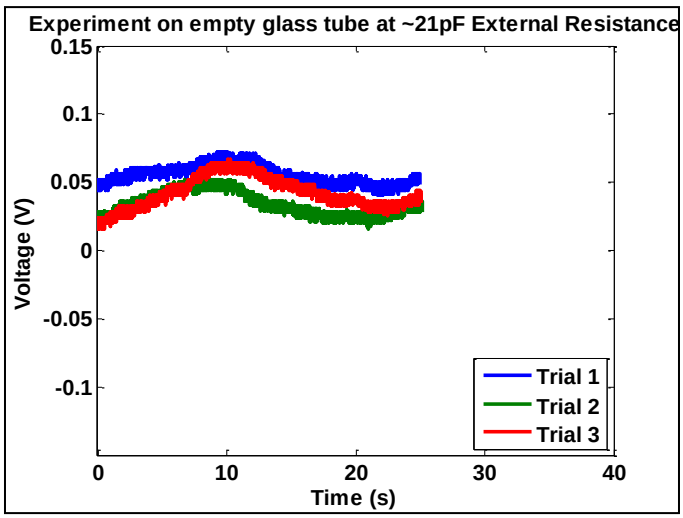

Figure 25: Experiment on an empty capillary tube with EM probe PF2: external capacitance = ~21 pF on Low Dynamic Reserve

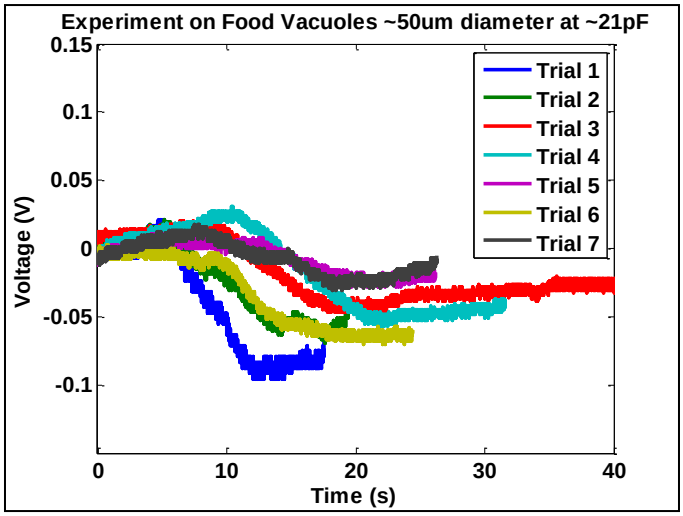

Figure 26: Experiment on food vacuoles ~50 μm in size with EM probe PF2: external capacitance = ~21 pF on Low Dynamic Reserve

Table 13: Initial Food Vacuole testing

Capacitance at ~21pF	Voltage Difference (mV)
Empty glass tube	16.2 ± 4.3
Food Vacuoles (~50 μm)	44.7 ± 25.7

The results presented in Figs. 25-26 and Table 13 show that there is some evidence that the food vacuoles may have been detected. However, it must be pointed out that under the conditions of these measurements, there was substantial noise and the entire circuit including the EM probe appeared to be sensitive to movement as far away as a foot away from the apparatus. Nevertheless, the data in Table 13 shows that there was signal when comparing measurements on the empty capillary tube and the capillary tube with the food vacuoles. Both the signal and the standard deviation are higher for the food vacuoles. This could be a result of the sample not positioned in the same location inside the probe for each trial. If the sample is at a different location within the probe, this will result in a seemingly random variation of the detected signal with each trial. While encouraging, these results must be repeated and perhaps so with a different coil design that is more sensitive than PF2. Moreover, these encouraging results must be verified by repeating these measurements with food vacuoles suspended in solution, as they would not be agglomerated *in vivo* as long as the parasite remains within the red blood cells.

5.5) Measurements on Iron oxide Particles using prototype PF2

In this section, measurements on iron oxide particles of different effective sizes are presented. The samples are prepared according to the procedure described in Chapter 4.

Table 14 provides the measured signals as the amount of iron oxide particles is varied. Based on this data, the sensitivity curves shown in Figs. 27-28 are constructed.

Table 14: Ordered results of iron particle testing using PF2

Sample	Mass (±0.2E-4 g)	Volume (μm^3)	Estimated Equivalent Diameter** (μm)	Voltage Difference (mV) ***
Particle	11.(8)E-4	149.9E+06	659.0	**545.473 ± 13.170**
7	5.(4)E-4	68.6E+06	507.8	**363.844 ± 7.965**
8	1.(2)E-4	15.2E+06	307.6	**133.282 ± 17.706**
9	1.(1)E-4	14.0E+06	298.8	**119.544 ± 5.754**
6	0.(8)E-4	10.2E+06	268.7	**41.393 ± 3.824**
3	0.(5)E-4	6.4E+06	229.8	**14.901 ± 2.444**
2	0.(2)E-4	2.5E+06	169.3	**6.571 ± 2.752**
5*	(0.05E-4)	0.6E+06	104.8	**4.711 ± 1.085**
1*	(0.04E-4)	0.5E+06	95.8	**4.694 ± 2.408**
4*	(0.04E-4)	0.5E+06	98.7	**2.521 ± 1.362**
Empty Tube	-	-	-	**1.718 ± 0.849**

*Volume estimated using microscope images
**Assumption: All particles combined equal perfect sphere
*** Measurements obtained from importing oscilloscope data into MatLab allowing for measurements to 3 decimal places (i.e. microvolts)

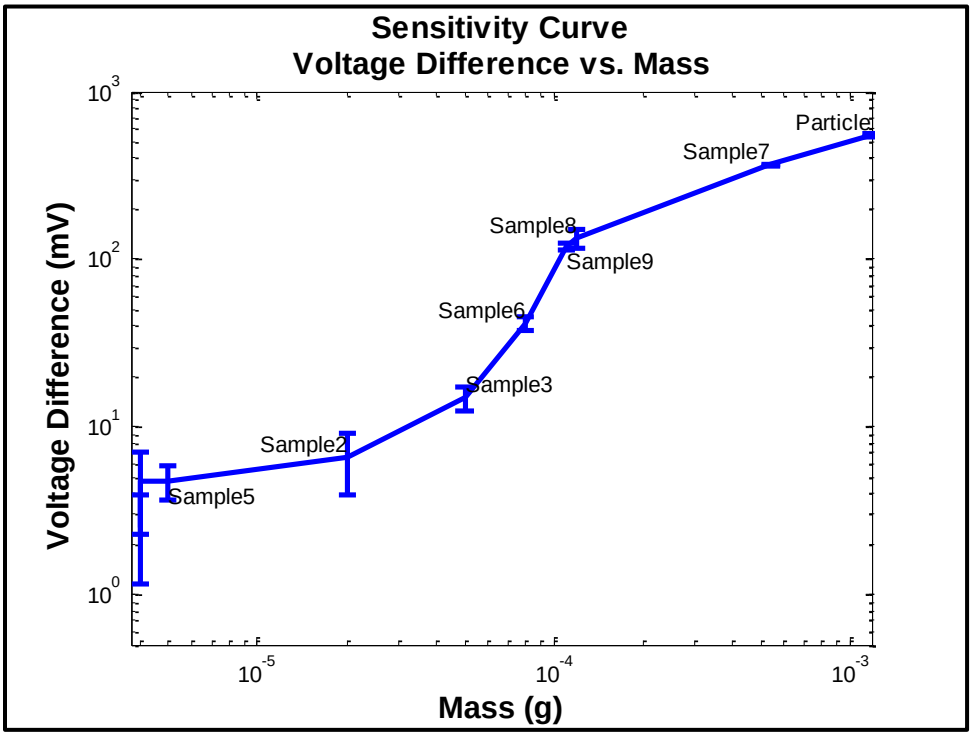

Figure 27: Sensitivity curve for iron particle voltage difference versus mass with EM probe PF2

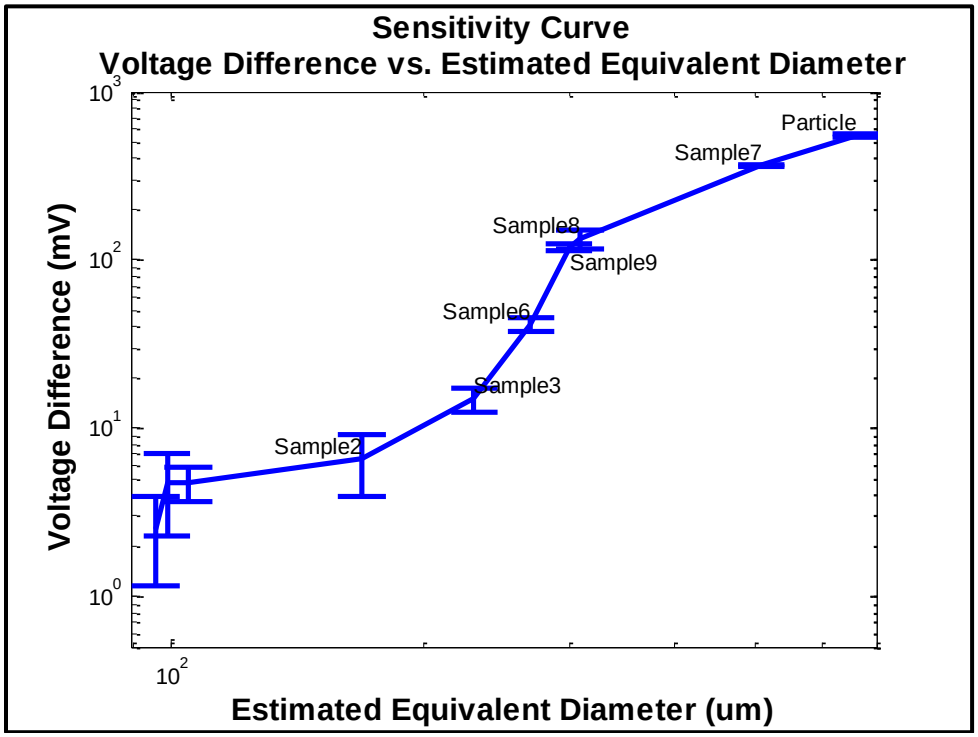

Figure 28: Sensitivity curve for iron particle voltage difference versus estimated equivalent diameter with EM probe PF2

The results presented in Table 14 and Figs. 27-28 show as expected that the signal drastically decreases as the mass (and equivalent particle diameter) decrease. It is important to point out that not all samples had evenly distributed particles, as can be seen in the microscope images in Appendix A. In some samples, the particles were much more spread out than in others. Sample 7 in particular, is a sample that is spread throughout a capillary tube, and the resulting signal is well over half the signal obtained from the solid 659 μm particle even though the volume of Sample 7 is not quite half that of the solid 659 μm particle. This suggests that perhaps a more spread out distribution might yield a larger signal, and may in fact mimic the flow of infected erythrocytes *in vivo*. This result also suggests that performing measurements on food vacuoles in solution may be more relevant for the field application rather than the measurements on agglomerated iron oxide particles.

The results presented in this section do show that particles on the scale of microns can be detected and the non-invasive approach of detecting malaria presented in this thesis is feasible. Moreover, the sensitivity curves imply that if sufficient control is attained over signal to noise, then iron-rich particles much smaller than the ones considered in this thesis can be detected. However, while the sensitivity of the probe can be increased by reducing the sensitivity setting on the lock-in amplifier from 2mV/V down to 20μV/V, the noise may just be too large to collect any signal.

Summary, Conclusions, and Recommendations for Further Work

In this research, an EM probe for detecting iron-rich particles on the scale of microns and remnant food vacuoles from PF infected blood has been developed. Measurements on different sized iron oxide particles demonstrate that detecting iron-rich islands on the scale of microns can indeed be detected. Measurements on actual food vacuoles isolated from human blood are encouraging and indicate despite the high noise level in the signal, may be feasible *in vivo*. This work has also identified design changes that could be made to the next generation of EM probes for detecting malaria-infected red blood cells.

An important parameter that has been identified is the distance between the iron-rich target and the sensing surface of the EM probe. When comparing initial measurements with PF1 with those with PF2, the further the probe is away from the sample, the lower the detected signal and thus the lower the sensitivity of the probe. This is important to remember when future work or in re-designing the next generation EM probe in which the sample will be placed inside the coil, simulating a finger inserted into an EM probe.

It has also been shown in this work that the probe can be optimized through changing external capacitance and modifying the ballast resistance in the circuit. By continuing to optimize these and other parameters, greater sensitivity can be attained with an accompanying reduction in noise.

Initial experiments on food vacuoles have been promising when changing the external capacitance. However, further measurements on food vacuoles in solution must be

completed before definitive conclusions can be drawn regarding translating this technology into the field.

It is pertinent to relate the measurements reported in this thesis to expected requirements for detecting malaria *in vivo*, in order to explore feasibility of reducing the method described in this thesis to practice. A 5% level of parasitemia (i.e. 5% of red blood cells (RBC) infected with PF) results in a patient exhibiting symptoms [15]. Since the typical concentration of RBCs in human blood is at least $4x10^9$ cells/mL, and assuming a capillary of 1 mm length, and 10 μm diameter [16], the number of cells accessible over a 2 second period would be 314 cells per capillary. At a level of 5% parasitemia, that amounts to about 16 infected RBCs per capillary. The average density of capillaries in the middle finger has been measured [17] and can be taken to be on the order of about 75 per mm^2. Therefore, in a field of about 1 cm^2, there would be ~7500 capillaries and ~ $1.2x10^5$ infected RBCs. Assuming that each infected RBC contains 1 food vacuole, that is a minimum of $1.2x10^5$ food vacuoles (taken to be 1 μm in size, an equivalent diameter of $1.2x10^5$ μm) that must be detected. This is equivalent to an iron-rich hemozoin volume of $6x10^{-8}$ cm^3 ($6x10^4$ $(\mu m)^3$). Taking the density of hemozoin to be 1.49 g/cm^3 [18], that amounts to an equivalent mass of ~$9x10^{-8}$ g or about 100 ng over the 1 cm^2 detection area. This is about an order of magnitude (40 times) smaller than the smallest iron oxide particle as can be seen from the data in Table 14. However, 100 ng is exactly what was detected (albeit with a large standard deviation) as can be seen from Table 13 (50 μm effective diameter corresponds to $6.5x10^{-8}$ cm^3 or an effective hemozoin mass of ~10^{-7} g or 100 ng). Therefore, the measurement of PF *in vivo* appears feasible by these order of magnitude

arguments, despite the fact that it is at or slightly beyond the limit of sensitivity based on the data presented in this thesis.

On the positive side, the type of EM detection described in this thesis will prove to be easy to manufacture and inexpensive. This is an important aspect of the research presented here. Further refinement of the coil will result in greater sensitivity in making the end-goal of this research a reality.

Future work should begin with measurements using the current coil design in its optimized state on a solution of food vacuoles. If experimental evidence shows that the food vacuoles in liquid suspensions can be detected using the current EM probe design, then the next step should involve *in vitro* measurements on PF infected blood in the same capillary tubes used in this research.

There is considerable potential for attaining greater sensitivity. Techniques studied in the Applied Physics Laboratory on detecting cancer can be used to further optimize the EM probe. Refining the EM probe so that a 1 by 1 EM probe is optimized before repeating measurements on food vacuoles or PF infected blood is important.

Appendix

Appendix A

Iron Particle Samples under a compound microscope:

Note: All samples under 100x zoom are just 1.3 millimeters of the whole sample

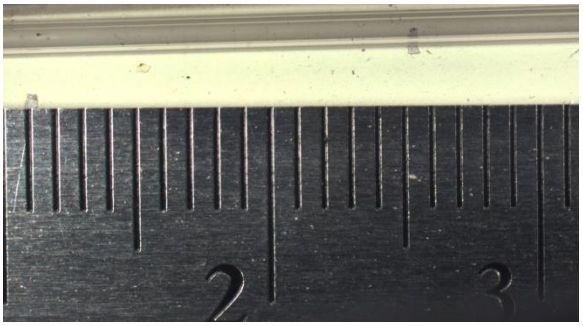

Sample 1 – 35x Magnification
(all individual scale marks are millimeters)

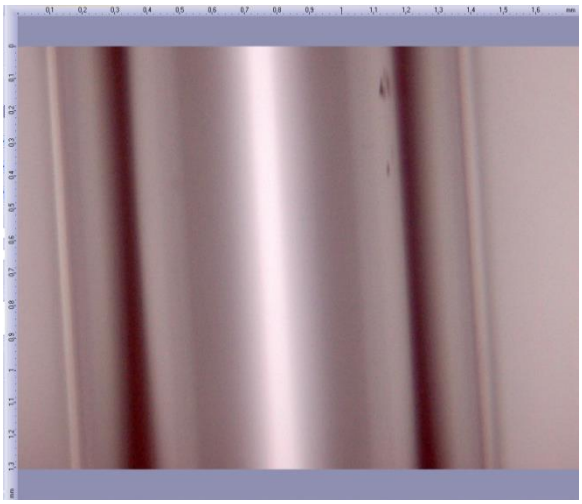

Sample 1 – 100x Magnification

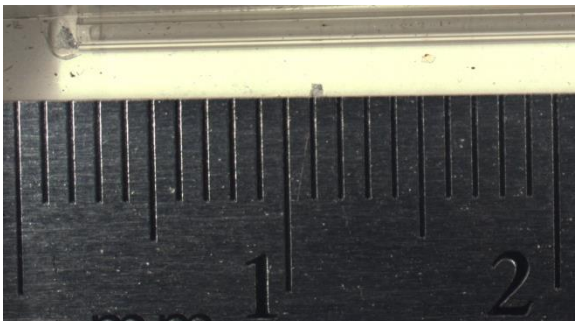

Sample 2 – 35x Magnification
(all individual scale marks are millimeters)

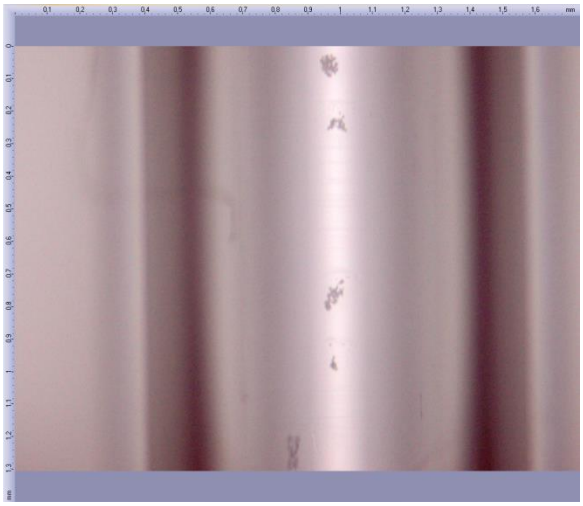

Sample 2 – 100x Magnification

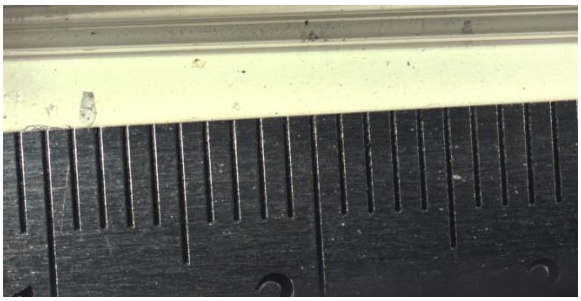

Sample 3 – 35x Magnification
(all individual scale marks are millimeters)

Sample 3 – 100x Magnification

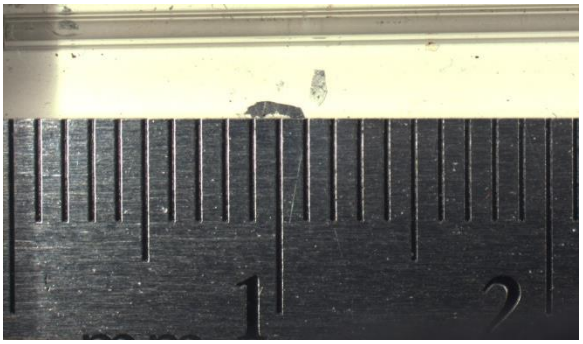

Sample 4 – 35x Magnification
(all individual scale marks are millimeters)

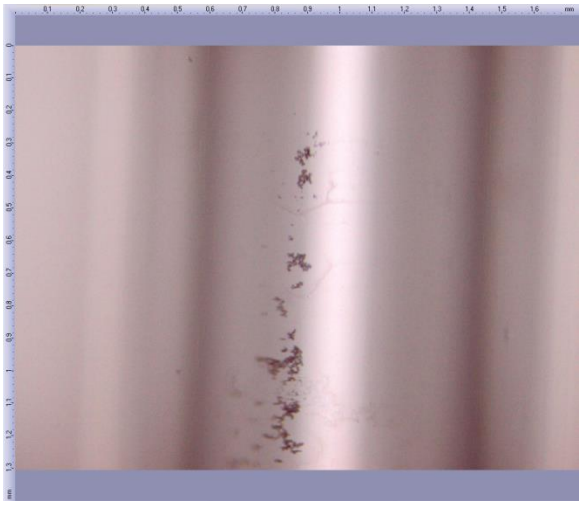

Sample 4 – 100x Magnification

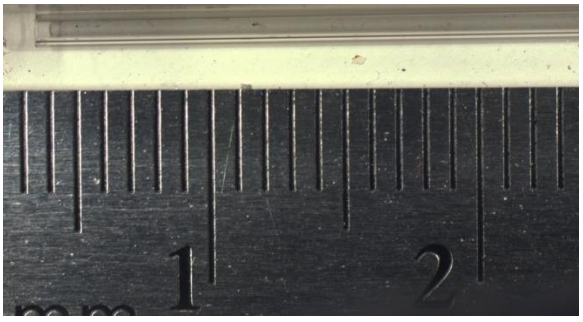

Sample 5 – 35x Magnification
(all individual scale marks are millimeters)

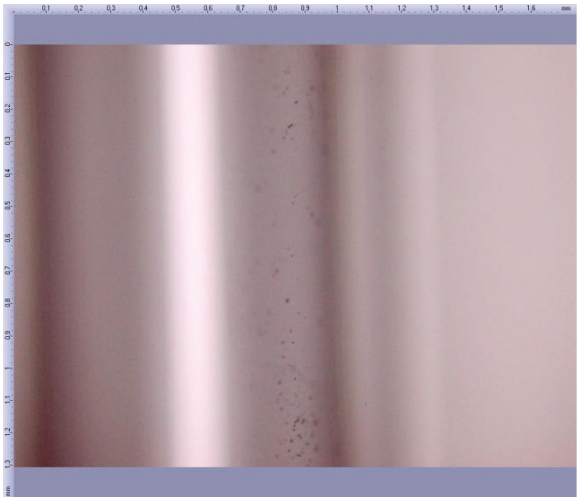

Sample 5 – 100x Magnification

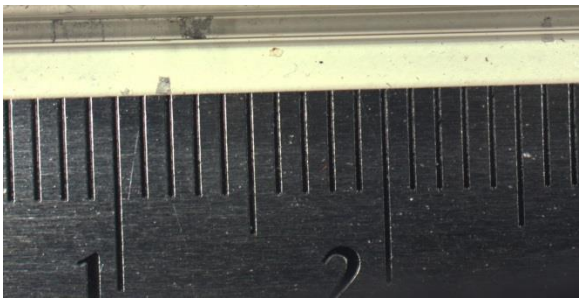

Sample 6 – 35x Magnification
(all individual scale marks are millimeters)

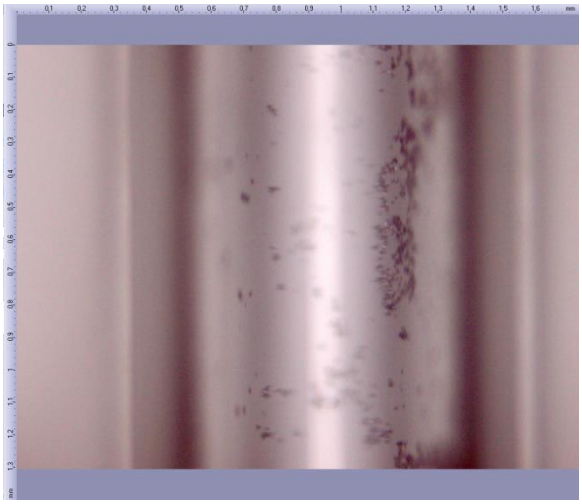

Sample 6 – 100x Magnification

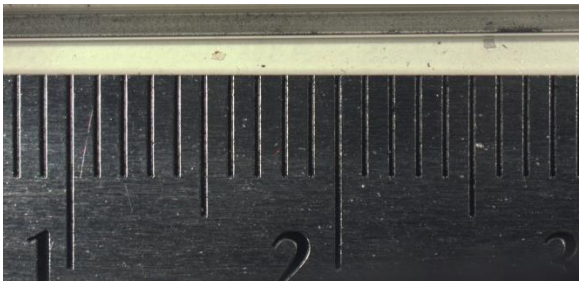

Sample 7 – 35x Magnification
(all individual scale marks are millimeters)

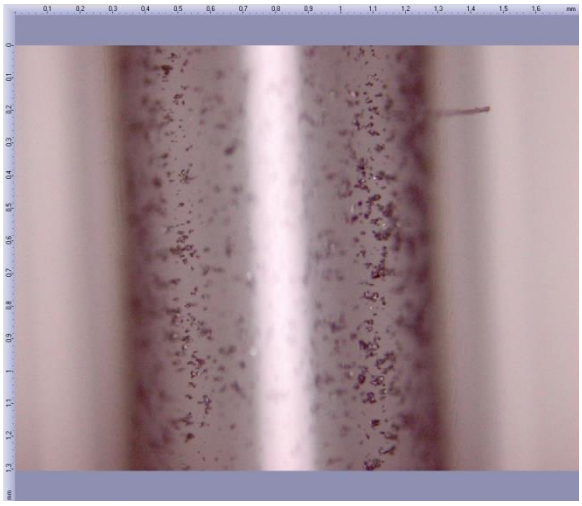

Sample 7 – 100x Magnification

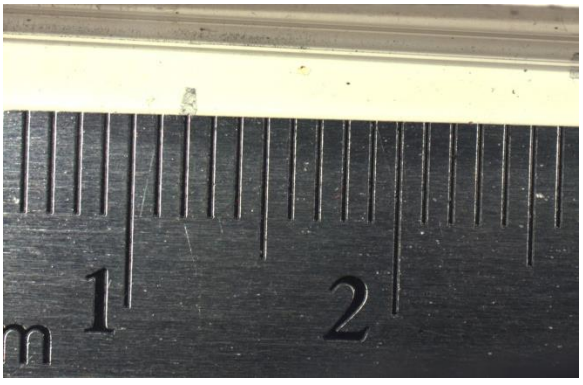

Sample 8 – 35x Magnification
(all individual scale marks are millimeters)

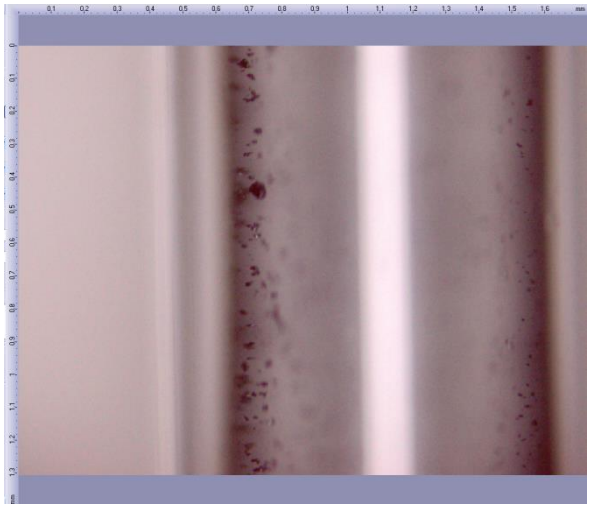

Sample 8 – 100x Magnification

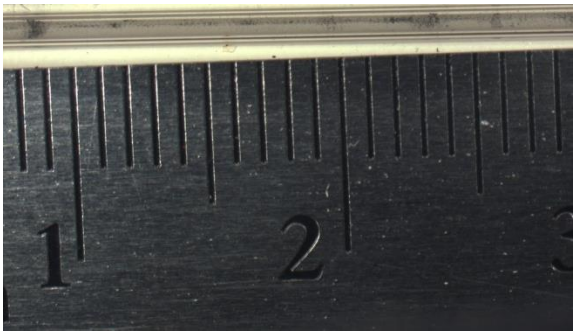

Sample 9 – 35x Magnification
(all individual scale marks are millimeters)

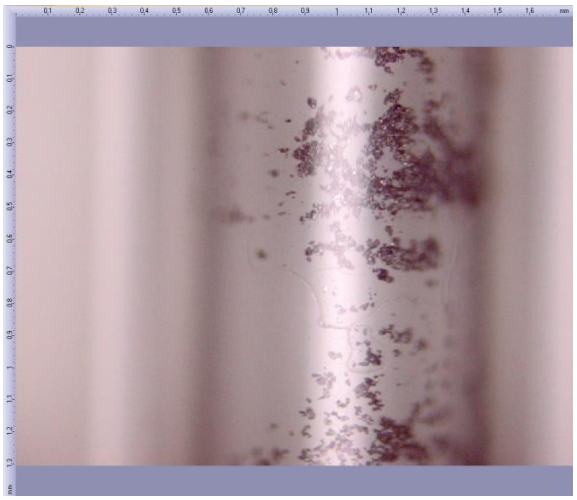
Sample 9 – 100x Magnification

Large Particle Sample – No magnification
(all individual scale marks are millimeters)

Appendix B

PF2 Ballast Resistance Results – Oscilloscope Traces

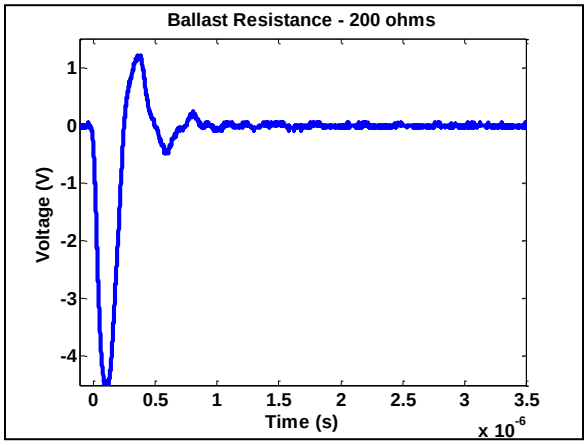

200 Ω Ballast Resistance Oscilloscope Trace

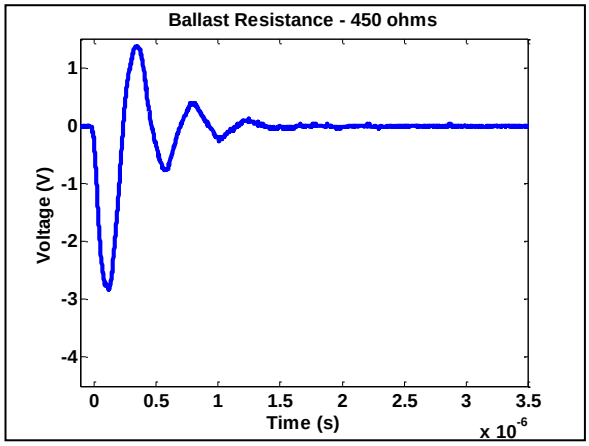

450 Ω Ballast Resistance Oscilloscope Trace

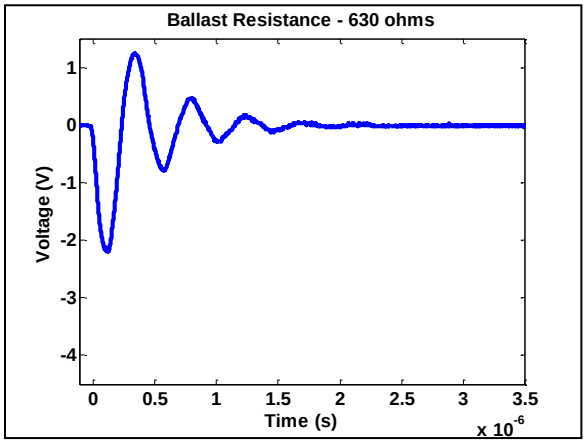

630 Ω Ballast Resistance Oscilloscope Trace

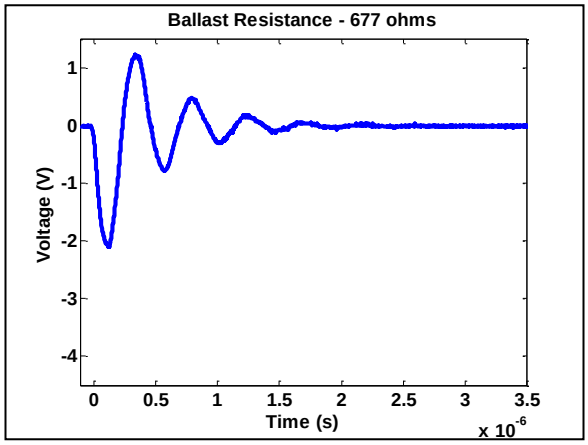

677 Ω Ballast Resistance Oscilloscope Trace

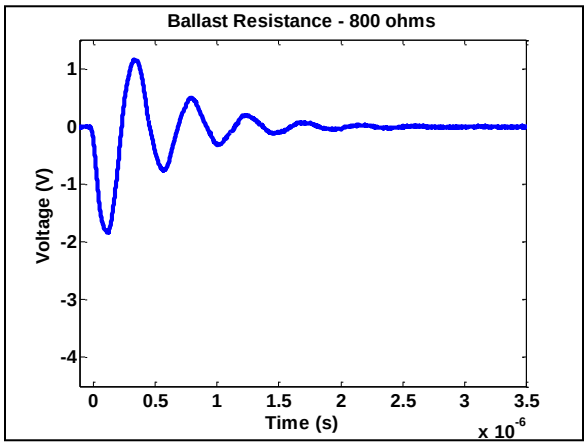

800 Ω Ballast Resistance Oscilloscope Trace

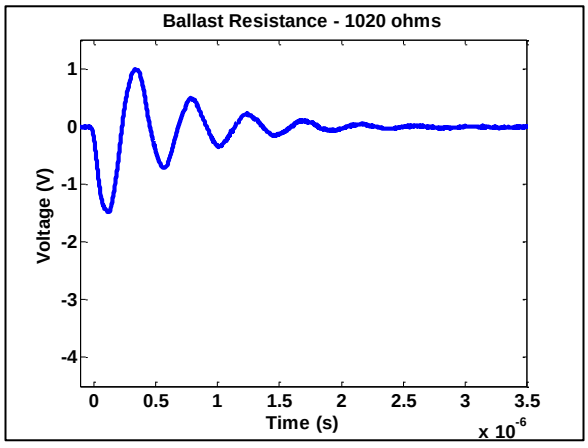

1020 Ω Ballast Resistance Oscilloscope Trace

Appendix C

PF2 External Capacitance Results:

390 Ω Ballast Resistance

Capacitance (pF)		V	mV *absolute value	Ref. on LIA (degrees)
0	Average Voltage Difference	0.07868	78.6755	-157.7
	Standard Deviation	0.00169	1.6909	
10	Average Voltage Difference	0.01064	10.6423	-155.8
	Standard Deviation	0.00047	0.4714	
20	Average Voltage Difference	-0.04618	46.1797	-164.3
	Standard Deviation	0.00166	1.6604	
30	Average Voltage Difference	-0.01170	11.6971	-157.8
	Standard Deviation	0.00151	1.5114	
40	Average Voltage Difference	0.00215	2.1460	-156.4
	Standard Deviation	0.00589	5.8908	
50	Average Voltage Difference	0.02040	20.3957	-155.8
	Standard Deviation	0.00349	3.4900	
60	Average Voltage Difference	-0.03950	39.4978	-155.4
	Standard Deviation	0.00420	4.1964	
70	Average Voltage Difference	-0.00521	5.2125	-154.1
	Standard Deviation	0.00691	6.9080	
80	Average Voltage Difference	-0.01205	12.0454	-153.5
	Standard Deviation	0.00528	5.2757	
90	Average Voltage Difference	-0.02967	29.6665	-152.5
	Standard Deviation	0.00924	9.2443	
100	Average Voltage Difference	-0.01781	17.8069	-151.7
	Standard Deviation	0.00155	1.5499	

800 Ω Ballast Resistance

Capacitance (pF)		V	mV *absolute value	Ref. on LIA (degrees)
0	Average Voltage Difference	0.01723	17.2297	-152.6
	Standard Deviation	0.00106	1.0619	
10	Average Voltage Difference	-0.19906	199.0646	-168.0
	Standard Deviation	0.01718	17.1835	
20	Average Voltage Difference	-0.05286	52.8597	-156.2
	Standard Deviation	0.00359	3.5943	
30	Average Voltage Difference	0.00392	3.9173	-154.5
	Standard Deviation	0.00221	2.2141	
40	Average Voltage Difference	-0.05097	50.9677	-153.5
	Standard Deviation	0.00476	4.7636	
50	Average Voltage Difference	-0.01212	12.1167	-151.4
	Standard Deviation	0.01060	10.6013	
60	Average Voltage Difference	-0.02132	21.3178	-150.8
	Standard Deviation	0.00874	8.7435	
70	Average Voltage Difference	-0.06378	63.7826	-148.9
	Standard Deviation	0.01145	11.4533	
80	Average Voltage Difference	-0.02771	27.7112	-147.7
	Standard Deviation	0.00384	3.8371	
90	Average Voltage Difference	-0.04232	42.3205	-144.0
	Standard Deviation	0.00120	1.2045	
100	Average Voltage Difference	0.03904	39.0351	-149.8
	Standard Deviation	0.00045	0.4511	

1020 Ω Ballast Resistance

Capacitance (pF)		V	mV *absolute value	Ref. on LIA (degrees)
0	Average Voltage Difference	-0.00012	0.1161	-151.1
	Standard Deviation	0.00531	5.3119	
10	Average Voltage Difference	-0.10668	106.6803	-162.0
	Standard Deviation	0.00763	7.6289	
20	Average Voltage Difference	-0.03813	38.1346	-154.4
	Standard Deviation	0.00221	2.2075	
30	Average Voltage Difference	0.00058	0.5788	-153.1
	Standard Deviation	0.00356	3.5551	
40	Average Voltage Difference	-0.04331	43.3106	-152.2
	Standard Deviation	0.00180	1.7989	
50	Average Voltage Difference	-0.00397	3.9670	-150.5
	Standard Deviation	0.00623	6.2283	
60	Average Voltage Difference	-0.04915	49.1517	-149.5
	Standard Deviation	0.00834	8.3435	
70	Average Voltage Difference	-0.04975	49.7487	-147.4
	Standard Deviation	0.00109	1.0864	
80	Average Voltage Difference	-0.03302	33.0249	-145.6
	Standard Deviation	0.00277	2.7661	
90	Average Voltage Difference	0.07388	73.8793	-144.0
	Standard Deviation	0.00051	0.5131	
100	Average Voltage Difference	0.02199	21.9928	-149.6
	Standard Deviation	0.00219	2.1942	

2200 Ω Ballast Resistance

Capacitance (pF)		V	mV *absolute value	Ref. on LIA (degrees)
0	Average Voltage Difference	-0.01648	16.4768	-155.3
	Standard Deviation	0.01029	10.2909	
10	Average Voltage Difference	-0.06485	64.8490	-153.2
	Standard Deviation	0.00553	5.5339	
20	Average Voltage Difference	0.00691	6.9091	-151.9
	Standard Deviation	0.00201	2.0125	
30	Average Voltage Difference	0.00301	3.0068	-164.2
	Standard Deviation	0.00043	0.4308	
40	Average Voltage Difference	-0.06675	66.7496	-156.8
	Standard Deviation	0.00275	2.7535	
50	Average Voltage Difference	-0.02346	23.4622	-155.2
	Standard Deviation	0.00268	2.6786	
60	Average Voltage Difference	0.00836	8.3570	-154.6
	Standard Deviation	0.00396	3.9588	
70	Average Voltage Difference	-0.08998	89.9779	-153.6
	Standard Deviation	0.01462	14.6245	
80	Average Voltage Difference	-0.12942	129.4194	-151.8
	Standard Deviation	0.00507	5.0733	
90	Average Voltage Difference	-0.05385	53.8484	-149.4
	Standard Deviation	0.00368	3.6848	
100	Average Voltage Difference	-0.04922	49.2180	-147.3
	Standard Deviation	0.00463	4.6340	

800 ohm ballast resistance– Low Dynamic Reserve

Capacitance (pF)		V	mV *absolute value	Ref. on LIA (degrees)
0	Average Voltage Difference	0.03821	38.2	-150.3
	Standard Deviation	0.00469	4.7	
10	Average Voltage Difference	-0.20702	207.0	-171.2
	Standard Deviation	0.00110	1.1	
20	Average Voltage Difference	-1.86789	1867.9	-150.3
	Standard Deviation	0.02724	27.2	
~21	Average Voltage Difference	-2.17302	2173.0	-148.4
	Standard Deviation	0.06434	64.3	

References

[1] Murray, Christopher JL, Lisa C. Rosenfeld, Stephen S. Lim, Kathryn G. Andrews, Kyle J. Foreman, Diana Haring, Nancy Fullman, Moshen Naghavi, Rafael Lozano, and Alan D. Lopez. "Global Malaria Mortality between 1980 and 2010: A Systematic Analysis." Global Malaria Mortality between 1980 and 2010: A Systematic Analysis 379.9814 (2012): 413-31. The Lancet. 4 Feb. 2012. Web. 2 Feb. 2013. <http://www.thelancet.com/journals/lancet/article/PIIS0140-6736%2812%2960034-8/fulltext#article_upsell>.

[2] Thompson, Mary, and Robert Brown. "Plasmodium falciparum Response to Oscillating Weak Magnetic Fields." (2011).

[3] "About Malaria." Johns Hopkins Bloomberg School of Public Health. N.p., n.d. Web. 1 Feb. 2013. <http://malaria.jhsph.edu/about_malaria/>.

[4] "Fact Sheet: Plasmodium Falciparum Malaria." Mvi: Malaria Vaccine Initiative, n.d. Web. 16 Mar. 2014. < http://www.malariavaccine.org/files/FS_Pfalciparum-Sept-2004_FINAL.pdf>.

[5] Thomas Akompong, Nafisa Ghori and Kasturi Haldar. “In Vitro Activity of Riboflavin against the Human Malaria Parasite Plasmodium falciparum” Antimicrob. Agents Chemotherapy. 2000, 44(1):88. DOI: 10.1128/AAC.44.1.88-96.2000.

[6] "Malaria Diagnosis (U.S.) – Rapid Diagnostic Test." *Centers for Disease Control and Prevention*. Centers for Disease Control and Prevention, 08 Feb. 2010. Web. 16 Mar. 2014. <http://www.cdc.gov/malaria/diagnosis_treatment/rdt.html>.

[7] "Malaria Diagnosis (U.S.) - Microscopy." Centers for Disease Control and Prevention. Centers for Disease Control and Prevention, 09 Nov. 2012. Web. 30 Jan. 2013. <http://www.cdc.gov/malaria/diagnosis_treatment/microscopy.html>.

[8] Milne, L. M., M. S. Kyi, et al. (1994)."Accuracy of routine laboratory diagnosis of malaria in the United Kingdom." J ClinPathol47(8): 740-2.

[9] McFerran Brock, J. L. (2009). *An Electromagnetic Method For Cancer Detection*. Columbus: PhD Dissertation, The Ohio State University.

[10] Sequin, E. K. (2009). *Imaging of Cancer in Tissues Using an Electromagnetic Probe*. Columbus: Master's Thesis, The Ohio State University.

[11] Wilson, M. L. (2011). *Design and Fabrication of an Electromagnetic Probe for Biomedical Applications.* Columbus: Master's Thesis, The Ohio State University.

[12] Zimmerman, Peter A., et al. "Diagnosis of malaria by magnetic deposition microscopy." *The American journal of tropical medicine and hygiene* 74.4 (2006): 568-572

[13] Newman, Dave M., John Heptinstall, Raphael J. Matelon, Luke Savage, M. Lesley Wears, Jamie Beddow, Martin Cox, Henk D.f.h. Schallig, and Petra F. Mens. "A Magneto-Optic Route toward the In Vivo Diagnosis of Malaria: Preliminary Results and Preclinical Trial Data." *Biophysical Journal* 95.2 (2008): 994-1000. Print.

[14] Ongagna-Yhombi, Serge Y., et al. "Improved assay to detect Plasmodium falciparum using an uninterrupted, semi-nested PCR and quantitative lateral flow analysis." *Malaria journal* 12.1 (2013): 74.

[15] Professor Mark Drew, Private communication, April 1, 2014.

[16] Stücker, M., et al. "Capillary blood cell velocity in human skin capillaries located perpendicularly to the skin surface: measured by a new laser Doppler anemometer." *Microvascular research* 52.2 (1996): 188-192.

[17] Antonios, Tarek FT, et al. "Structural skin capillary rarefaction in essential hypertension." *Hypertension* 33.4 (1999): 998-1001.

[18] Kapishnikov, Sergey, et al. "Oriented nucleation of hemozoin at the digestive vacuole membrane in Plasmodium falciparum." *Proceedings of the National Academy of Sciences* 109.28 (2012): 11188-11193.